ChemMedChem

Supporting Information

Andrographolide Derivatives Target the KEAP1/NRF2 Axis and Possess Potent Anti-SARS-CoV-2 Activity

Bianca Schulte, Maria König, Beate I. Escher, Sophie Wittenburg, Matic Proj, Valentina Wolf, Carina Lemke, Gregor Schnakenburg, Izidor Sosič, Hendrik Streeck, Christa E. Müller, Michael Gütschow, and Christian Steinebach*

Table of Content

Extended Method Section

Extraction of andrographolide from AP

Method A: AP leaves powder (250 g) was fed into a Soxhlet apparatus equipped with a cellulose extraction thimble. Extraction with MeOH (2000 mL) was carried out for 8 h. Evaporation of the solvent gave a green residue (approx. 7 g), which was triturated with toluene (3 × 100 mL) and crystallized from hexanes (200 mL). The green solid was filtered and dried in vacuo. It was subjected to column chromatography (5% MeOH in CH_2Cl_2). Andrographolide (1.63 g) and 14-deoxy-14,15-didehydroandrographolide (0.88 g) were obtained as colorless solids.

Method B: An alternative method employs extraction from commercially available AP dietary supplements. Ninety capsules containing 400 mg of a standardized AP extract (min. 10% andrographolide) were opened. The solid material (approx. 50 g) was poured into a 250 mL round-bottom flask. The material was treated with MeOH (200 mL) and stirred for 10 min at room temperature. The brown suspension was filtered, and the solid residue was macerated again with MeOH (200 mL). After the second filtration, the methanolic solution was evaporated to give the crude product (approx. 8 g), which was purified by column chromatography as described above. Andrographolide (4.68 g) and 14-deoxy-14,15-didehydro-andrographolide (0.82 g) were obtained as colorless solids.

logD measurements

The determination of the $logD_{7.4}$ values was performed by a chromatographic method as described previously.[1,2] The system was calibrated by plotting the retention times of six different drugs (atenolol, metoprolol, labetalol, diltiazem, triphenylene, permethrin) versus their literature known $logD_{7.4}$ in a calibration line ($R^2 = 0.99$). Subsequently, the mean retention times of the analytes were taken to calculate their $logD_{7.4}$ values with aid of the calibration line.

Plasma protein binding studies

Plasma protein binding (%PPB) was estimated by correlating the logarithmic retention times of the analytes on a CHIRALPAK HSA 50 × 3 mm, 5 µm column with the literature known %PPB values (converted into logK values) of the following drugs: warfarin, ketoprofen, budesonide, nizatidine, indomethacin, acetylsalicylic acid, carbamazepine, piroxicam, nicardipine, and cimetidine (for details, see Valko *et al.*[3]). Samples were dissolved in MeCN/DMSO 9:1 to achieve a final concentration of 0.5 mg/mL. The mobile phase A was 50 mM ammonium acetate adjusted to *p*H 7.4 with 10% NaOH, while mobile phase B was *i*PrOH. The flow rate was set to 1.0 mL/min, the UV detector was set to 254 nm, and the column temperature was kept at 30 °C. After injecting 3 µL of the sample, a linear gradient from 100% A to 30% *i*PrOH in 5.4 min was applied. From 5.4 to 18 min, 30% *i*PrOH was kept, followed by switching back to

100% A in 1.0 min and a re-equilibration time of 6 min. With the aid of the calibration line ($R^2 = 0.94$), the logK values of new substances were calculated and converted to their %PPB values.

Binding assays at the human adenosine A_{2A} receptor

Recombinant expression of the human adenosine A_{2A} receptor

CHO-S cells were diluted to 10^6 cells/mL (calculated for 250 mL) in Freestyle™ CHO Expression Medium (Gibco) in a total volume of 240 mL in 500 mL Optimum Growth™ flasks (Thomson). The human adenosine A_{2A} receptor sequence in pcDNA3.1(+) (312.5 µg) was dissolved in a total volume of 5 mL of Freestyle™ CHO Expression Medium (Gibco). In a separate tube an aqueous polyethylenimine solution (PEI, 25 kD, linear, from Polysciences, 937.5 µL, 1 µg/µL) was diluted in a total volume of 5 mL of Freestyle™ CHO Expression Medium (Gibco) and the solutions were gently shaken. Both solutions were subsequently mixed to a total volume of 10 mL and incubated for 15 min. The DNA-PEI complex was slowly added into the 500 mL flask containing the cells. The transfected cells were incubated for 24 h at 37 °C, 8% CO_2, on an orbital shaker platform, and harvested afterwards.

Membrane preparation

The harvested cells were resuspended in two tubes each containing 30 mL of 5 mM TRIS/2mM EDTA buffer. Cells were disrupted with an Ultraturrax homogenizer (IKA, Staufen, Germany, level 6, 2 x 15 s) on ice. The suspension was distributed into two centrifuge tubes and centrifuged for 10 min at 1.000*g*, 4 °C (Beckman Avanti JXN 26 centrifuge). The pellets were discarded and the supernatant was centrifuged for 60 min, at 7.000*g*, 4 °C. Then, the supernatant was discarded, and the pellets were resuspended in 10 mL (each tube) of 50 mM TRIS-HCl buffer *p*H 7.4 using an Ultraturrax homogenizer. The suspension was centrifuged again for 30 min, 48.000*g*, 4 °C. Finally, the pellets were resuspended and homogenized in 10 mL of 50 mM TRIS-HCl buffer, *p*H 7.4, and distributed into vials for storage at –80 °C until use.

Competition binding assays at the human adenosine A_{2A} receptor

Competition binding assays were performed using 5 nM [^{3}H]CGS-21680 (Perkin Elmer, Boston, USA) in a final volume of 400 µL containing 200 µL of 50 mM TRIS buffer, *p*H 7.4, 4 µL of the test compound dissolved in DMSO, 100 µL of membrane preparation in buffer, and 100 µl of radioligand solution in buffer. Non-specific binding was determined using the agonist NECA at a final concentration of 10 µM. Five different concentrations of andrographolide were tested (10 nM, 100 nM, 1 µM, 10 µM, and 100 µM). The incubation was performed at room temperature for 120 min. After the incubation, the assay mixture was filtered through GF/B glass fiber filters using a Brandel harvester (Brandel, Gaithersburg, MD, USA). Filters were washed four times (3−4 mL each) with ice-cold 50 mM TRIS-HCl buffer, *p*H 7.4. Then, filters were transferred into scintillation vials, incubated for 9 h with 2.5 mL of scintillation cocktail (TrisKem, Bruz, France), and counted in a liquid scintillation counter (Tricarb 2810TR) with a counting efficiency of ~53%. Three separate experiments were performed.

Mpro inhibition assay[4]

Freshly unfrozen recombinant His-tagged SARS-CoV-2 M^{pro} was assayed on a Fluostar Optima (BMG Labtech, Ortenberg, Germany) at 37 °C with an excitation wavelength of 360 nm and an emission wavelength of 460 nm. Black 96-well plates with a clear and flat bottom were purchased from Greiner Bio-One (Kremsmünster, Austria). The total volume per well was 50 µL. The assay buffer was 50 mM MOPS, *p*H 7.2 containing 10 mM NaCl, 1 mM EDTA and 0.01% Triton X-100. The substrate Boc-Abu-Tle-Leu-Gln-AMC was prepared as a 2.5 mM stock solution in DMSO. All test compounds were provided as 1 mM or 0.5 mM stock solutions in DMSO. The substrate stock solution was diluted 1+23 with assay buffer and pipetted into a well containing 1 µL of inhibitor solution. This mixture was tempered at 37 °C for 5 min. A volume of 1 µL of an enzyme-containing solution (0.4 µg/µL His-tagged M^{pro} in storage buffer) was diluted 1+24 with assay buffer and added to start the reaction which was followed for 10 min. The final protein concentration was 8 ng/µL of His-tagged M^{pro}. The final substrate concentration was 50 µM (= 1.03 K_m) and the final DMSO content was 4%. The product formation rate of the uninhibited control was set to 100%, to which the inhibitory activity of test compounds was related.

Supplementary Tables and Figures

Table S1. AREc32 NRF2 assay descriptors.

Cmpd	**IC_{10}**[a] (µM)	**$EC_{IR1.5}$**[b] (µM)	**$IC_{10,baseline}$**[c] (µM)	**Toxic ratio, TR**[d]
Andrographolide (**1**)	95	4.9	798	8.4
14-Deoxy-14,15-didehydroandrographolide (**2**)	130	23	445	3.4
9	491	2.3	798	1.6
11	n.e.[e]	n.e.	754	n.d.[f]
16a	165	4.6	334	2.0
16b	545	51	445	0.8
16c	52	3.9	2640	51

[a] Inhibitory concentration for 10% reduction of cell confluency. [b] Effect concentratio causing an induction ratio (IR) of 1.5 to 50% over control IR of 1, see equation (2). [c] Baseline toxicity predicted by a QSAR method, see equation (3).[5] [d] Measure of enhanced cytotoxicity. Toxicity ratio (TR) ≥ 10, specific or reactive toxicity; TR < 10, baseline toxicant.[6] See equation (5). (e) No effect. (f) Not determined.

Equations used for the calculation of AREc32 NRF2 assay descriptors:[5,7,8]

$$IC_{10} = \frac{10\%}{\text{slope}} \quad (1)$$

$$EC_{IR1.5} = \frac{0.5}{\text{slope}} \quad (2)$$

$$\log\left(\frac{1}{IC_{10,baseline}}\right) = 4.01 \times \left(1 - e^{-0.281 \times \log D_{7.4}}\right) + 1.25 \quad (3)$$

$$SR = \frac{IC_{10}}{EC_{IR1.5}} \quad (4)$$

$$TR = \frac{IC_{10,baseline}}{IC_{10}} \quad (5)$$

Table S2. Results from the NAC/glutathione (GSH) HPLC-MS assay. No adducts with glutathione (GSH) or NAC were detected for **1**, **2** and **4.**

Cmpd	***m/z*, calcd**	***m/z*, found**	**t_R** (min)	**GSH adduct**	**t_R** (min)	**NAC adduct**	**t_R** (min)
1	350.21	$[M+HCO_2H]^-$	4.3	n.d.[a]		n.d.	
2	332.20	$[M–H_2O+H]^+$	5.6	n.d.		n.d.	
4	505.32	$[M+H]^+$	8.5	n.d.		n.d.	
NSC8368[b]	202.99	$[M+H]^+$		474.10	3.5	n.d.[d]	

[a] Not detected. [b] 2-Chloro-*N*-(3-chlorophenyl)acetamide was used as control. [c] Not determined.

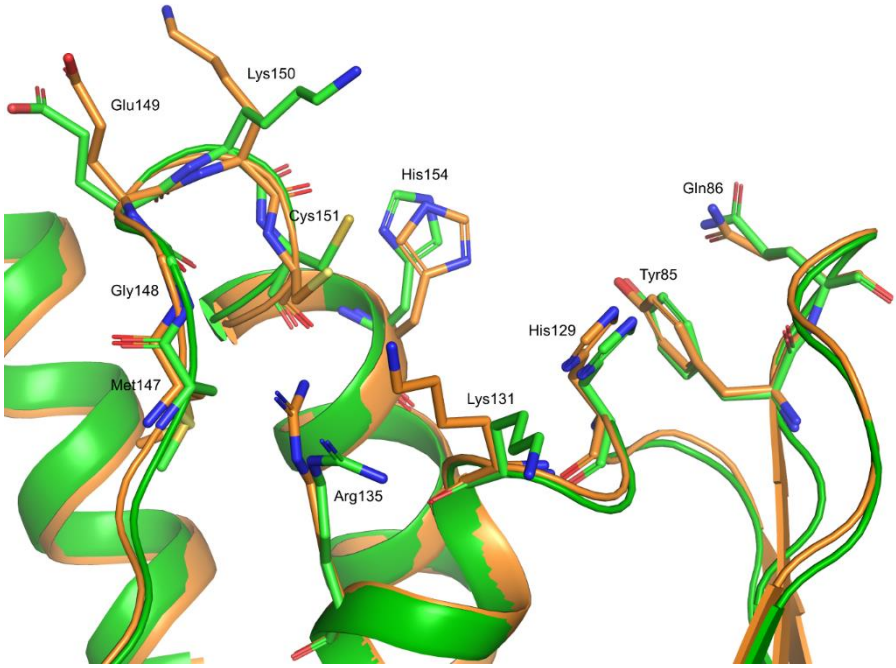

Figure S1. Binding site alignment of the BTB domain of KEAP1 co-crystallized with CDDO (4CXT, green, CDDO not shown) and the apo form of BTB domain of KEAP1 (4CXI, orange).

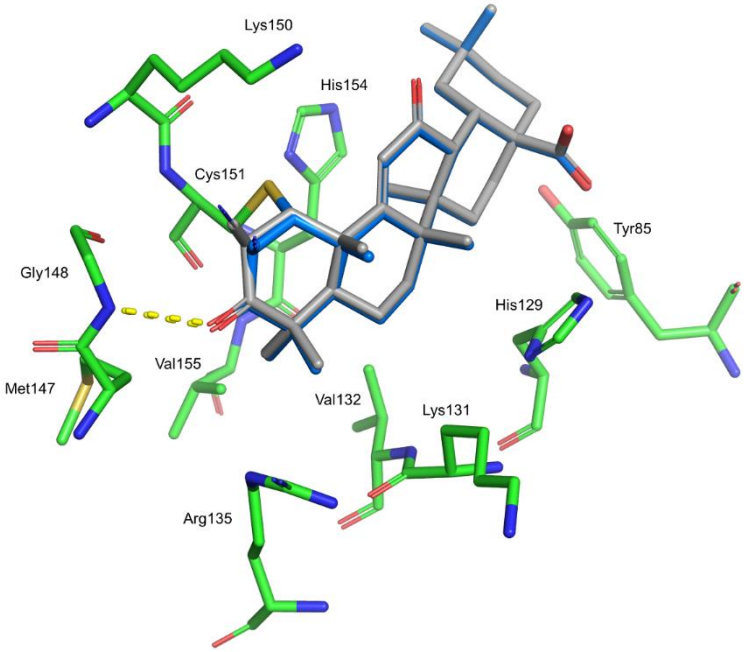

Figure S2. Re-docking of CDDO (blue) into the BTB domain of KEAP1 (PDB: 4CXT, green). The docking pose matches the crystal pose of CDDO (gray), RMSD = 0.61 Å. Dashed yellow lines represent hydrogen bonds.

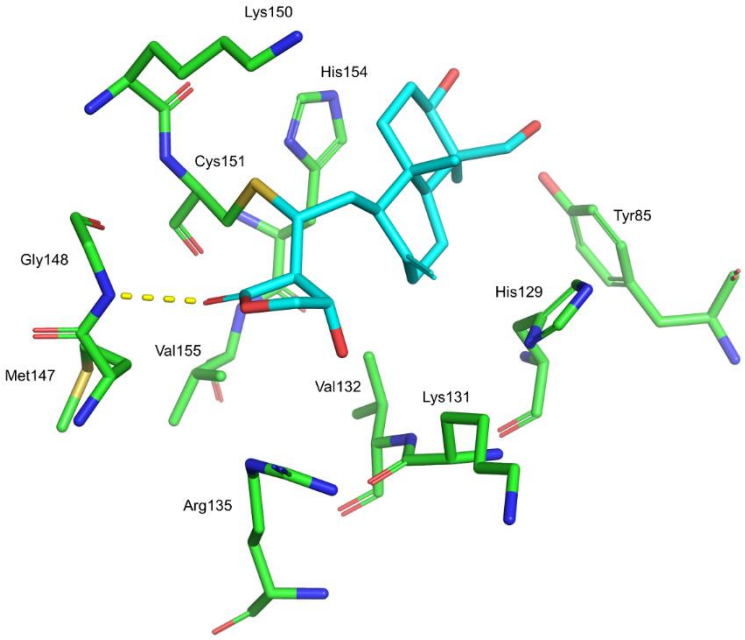

Figure S3. Covalent docking of andrographolide (**1**, cyan) into the BTB domain of KEAP1 (PDB: 4CXT, green). Dashed yellow line represents a hydrogen bond.

Cmpd 1

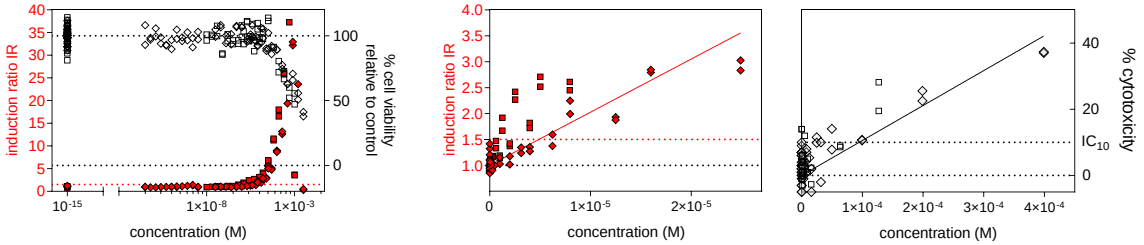

Cmpd 2

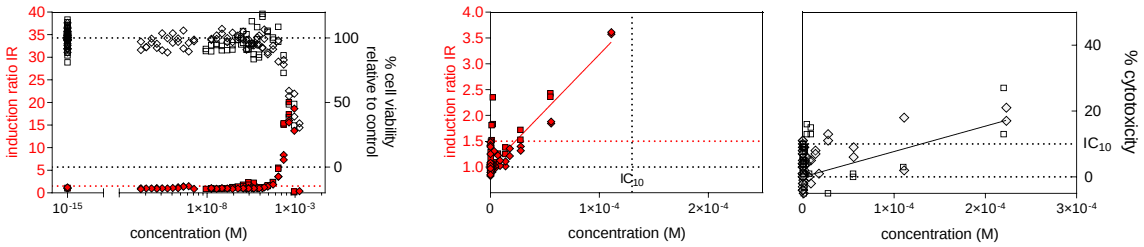

Cmpd 9

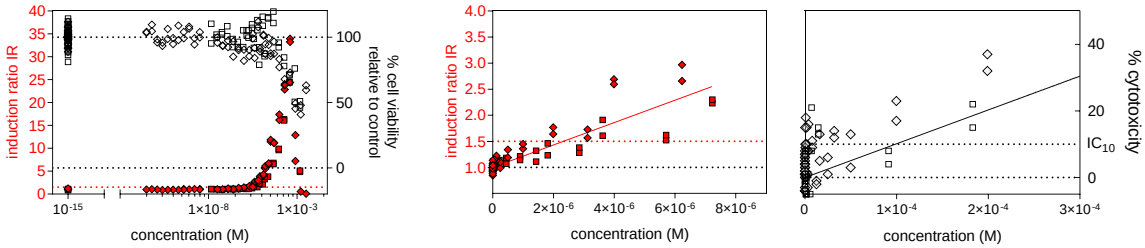

Cmpd 11

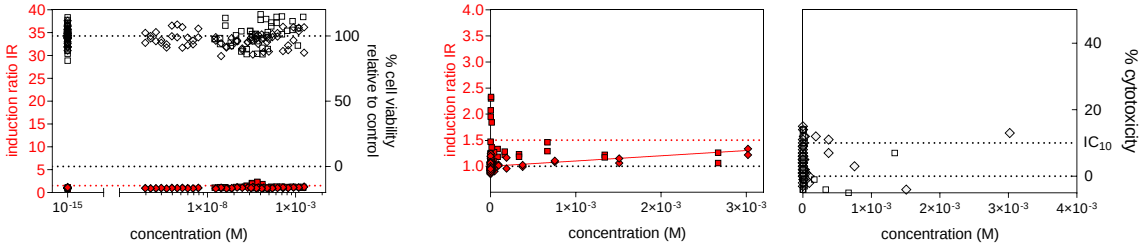

Cmpd 16a

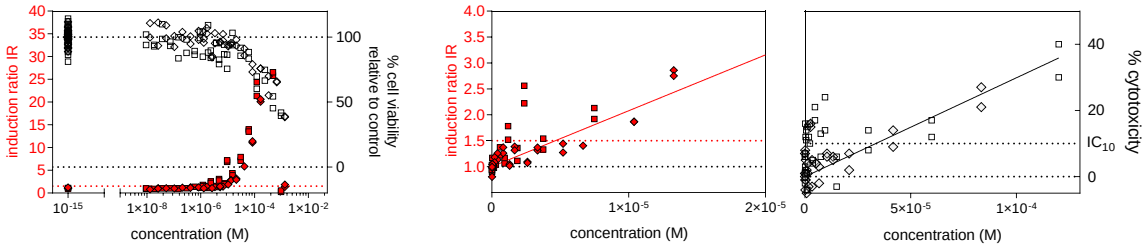

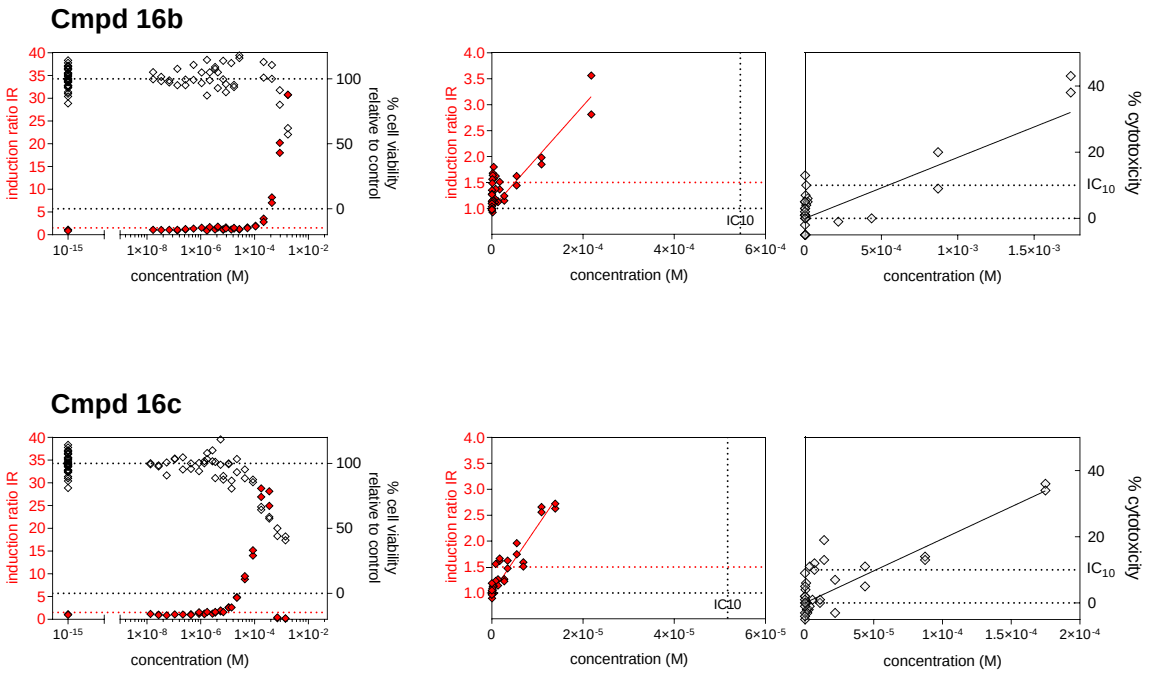

Figure S4. Concentration-effect curves for andrographolide and related semi-synthetic compounds. The left plot shows all data for IR (see equation 4) in red on the left y-axis and percentage cell viability relative to unexposed cells is plotted on the right y-axis. The right plots show cell viability converted to % cytotoxicity (% cytotoxicity = 100% – % cell viability) plotted for the linear portion of the concentration-response curves up to 40% cytotoxicity to derive the IC_{10}. Only concentrations below IC_{10} and in the linear range of the concentration response curves (up to IR 4) were then plotted in the middle plot to derive the $EC_{IR1.5}$. Details on the concentration-response modelling are given in Escher *et al.*, 2018.[9] Different symbols represent independent repeats of experiments on different days, **16b** and **16c** were run several times but on the same plate.

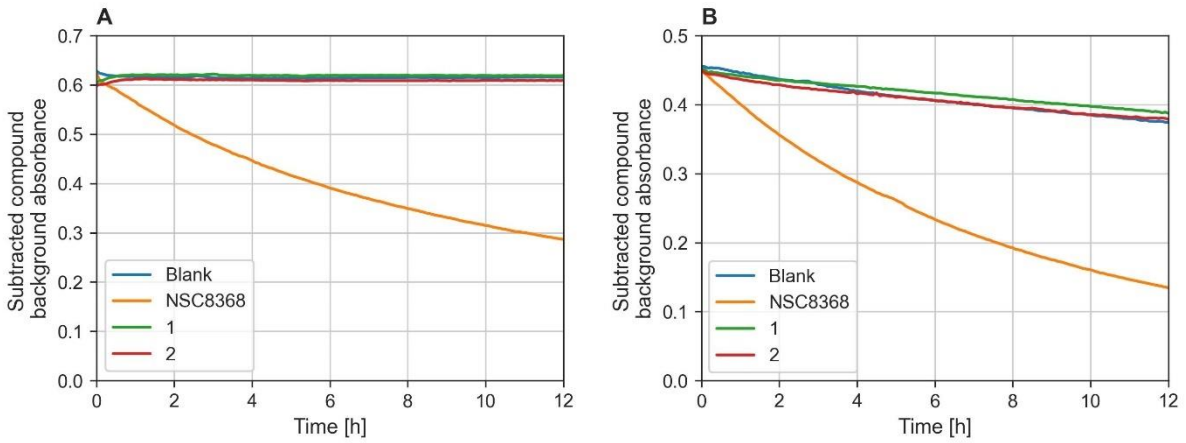

Figure S5. Results of the spectrophotometric Ellman's assay. When the cysteine thiol surrogate TNB^{2-} is incubated with **1** or **2** (A) in the presence or (B) in the absence of TCEP, no significant depletion of TNB^{2-}

is observed compared to the blank. 2-Chloro-*N*-(3-chlorophenyl)acetamide (NSC8368) was used as a control.

A

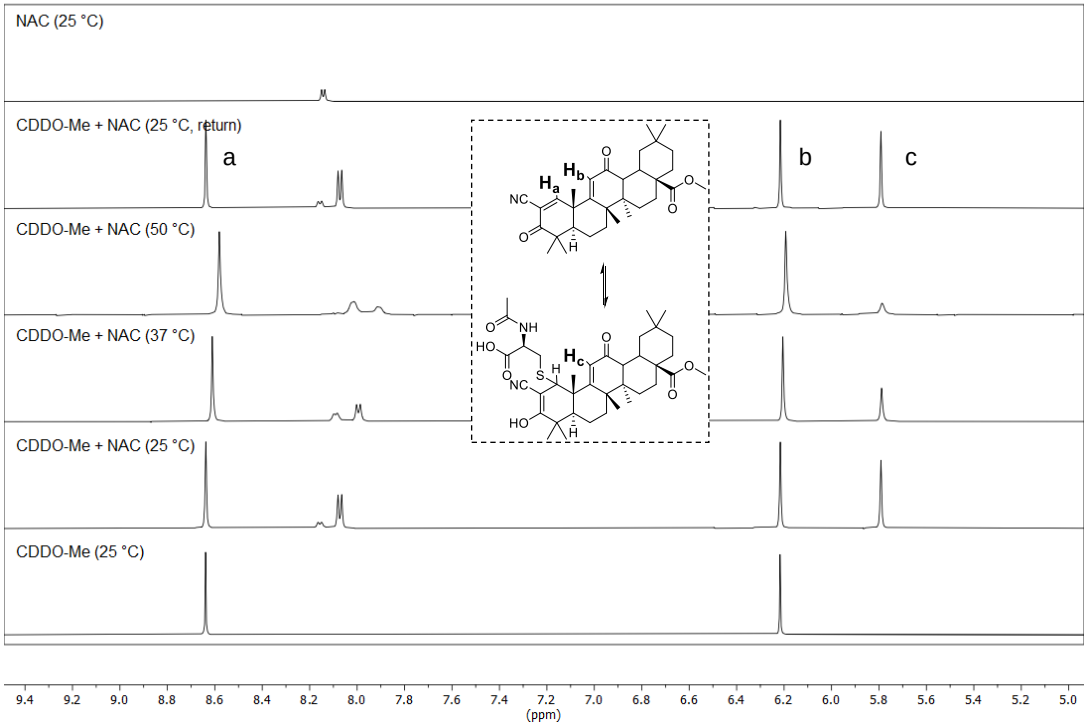

B

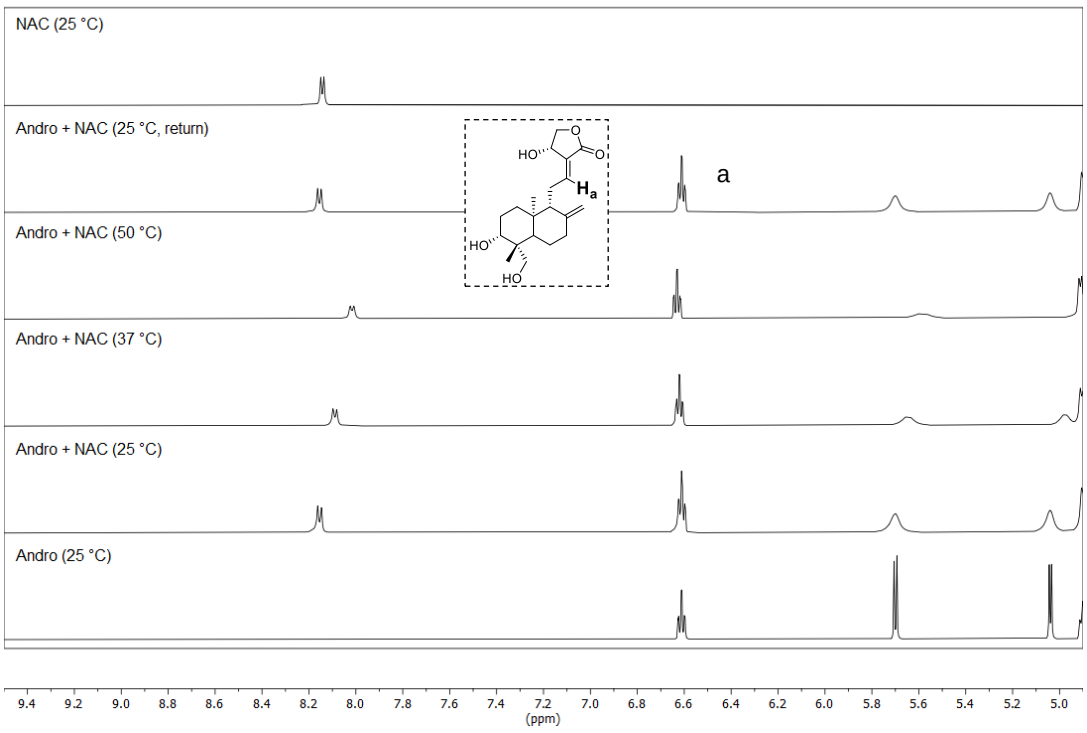

Figure S6. ^{1}H NMR evidence for a reversible thiol addition. CDDO-Me (A) or andrographolide (B) were incubated with one equivalent of *N*-acetylcysteine (NAC). In the case of CDDO-Me, an additional peak at 5.8 ppm occurs for the vinylic proton H_b, which is due to the shielding effect of the sulfur attacking the carbon atom where H_a is bound.[10] No modifications of peak H_a were observed after addition of NAC and temperature increase in the case of andrographolide.

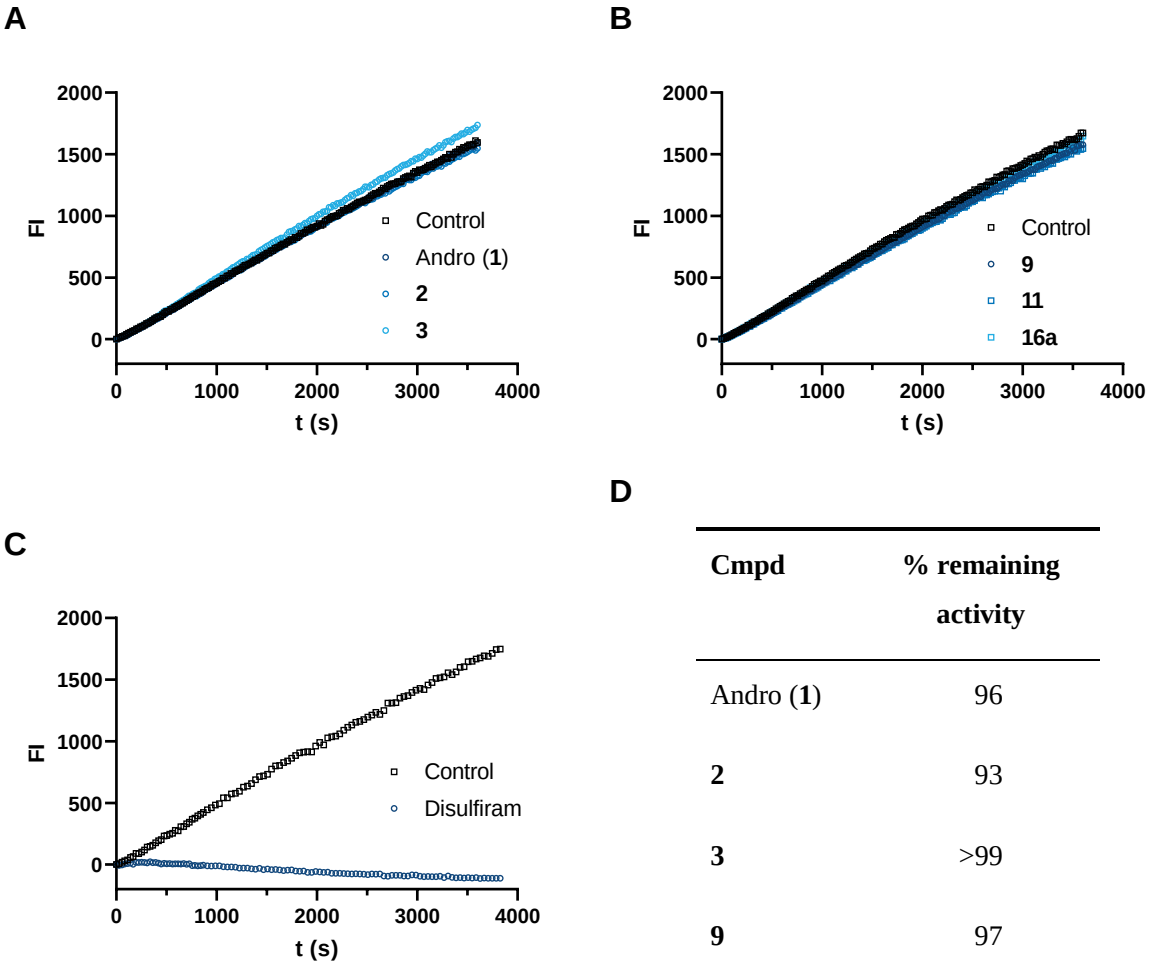

D

Cmpd	% remaining activity
Andro (**1**)	96
2	93
3	>99
9	97
11	99
16a	>99

Figure S7. Results of the SARS-CoV-2 M^{pro} inhibition assay. Product formation of Boc-Abu-Tle-Leu-Gln-AMC (50 µM) in the presence of His-tagged SARS-CoV-2 M^{pro} at 37 °C for 60 min. (A) Product formation in the presence of andrographolide (**1**), 14-deoxy-14,15-didehydroandrographolide (**2**) and 14-deoxy-11,12-didehydro-andrographolide (**3**) at a concentration of 20 µM in comparison to a control reaction. (B) Product formation in the presence of the semisynthetic AP derivatives **9**, **11**, and **16a** at a concentration of 20 µM in comparison to a control reaction. (C) Product formation of the reported SARS-CoV-2 M^{pro} inhibitor disulfiram at a concentration of 10 µM in comparison to a control reaction. (D) Mean of the remaining activity of andrographolide as well as its natural and semi-synthetic derivatives determined in two individual measurements at a single concentration of 20 µM. Values were calculated by end point determination and were compared to the mean of two controls.

Spectroscopic Details of Andrographolide Derivatives

Andrographolide (1)[11]

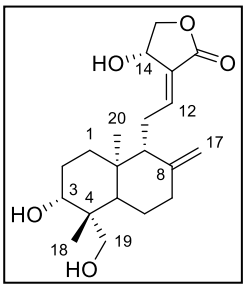

^{1}H NMR (600 MHz, DMSO-d_6) δ 0.65 (s, 3H, 20-H), 1.08 (s, 3H, 18-H), 1.17 – 1.24 (m, 2H, 5-H, 1-H), 1.29 – 1.39 (m, 1H, 11-H), 1.59 – 1.76 (m, 4H, 2-H, 6-H, 1-H‘), 1.85 (dd, *J* = 3.4, 11.0 Hz, 1H, 9-H), 1.88 – 1.96 (m, 1H, 7-H), 2.28 – 2.34 (m, 1H, 7-H‘), 2.40 – 2.54 (m, 2H, 6-H‘, 11-H‘), 3.19 – 3.29 (m, 2H, 3-H, 19-H), 3.83 (dd, *J* = 2.9, 11.0 Hz, 1H, 19-H‘), 4.02 (dd, *J* = 2.1, 9.9 Hz, 1H, OH), 4.11 (dd, *J* = 2.9, 7.5 Hz, 1H, 15-H), 4.38 (dd, *J* = 6.1, 9.9 Hz, 1H, 15-H‘), 4.62 (d, *J* = 1.7 Hz, 1H, 17-H), 4.80 (q, *J* = 1.6 Hz, 1H, 17-H‘), 4.90 (tt, *J* = 1.9, 6.1 Hz, 1H, 14-H), 5.02 (d, *J* = 4.8 Hz, 1H, OH), 5.69 (d, *J* = 6.1 Hz, 1H, OH), 6.61 (td, *J* = 1.8, 6.9 Hz, 1H, 12-H); **^{13}C NMR** (151 MHz, DMSO-d_6) δ 14.89 (C-20), 23.22 (C-18), 24.11 (C-6, C-11), 28.05 (C-2), 36.67 (C-1), 37.66 (C-7), 38.74 (C-10), 42.44 (C-4), 54.54 (C-5), 55.64 (C-9), 62.79 (C-19), 64.67 (C-14), 74.46 (C-15), 78.60 (C-3), 108.38 (C-17), 129.14 (C-13), 146.42 (C-12), 147.76 (C-8), 170.08 (CO).

14-Deoxy-14,15-didehydroandrographolide (2)[12]

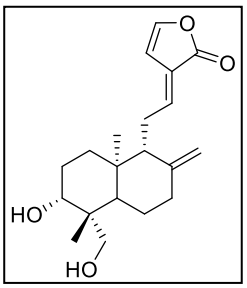

^{1}H NMR (500 MHz, DMSO-d_6) δ 0.75 (s, 3H), 1.09 (s, 3H), 1.10 – 1.21 (m, 2H), 1.28 – 1.35 (m, 1H), 1.32 – 1.46 (m, 1H), 1.52 – 1.66 (m, 2H), 1.66 – 1.76 (m, 1H), 1.92 – 2.02 (m, 1H), 2.29 – 2.40 (m, 2H), 3.18 – 3.31 (m, 2H), 3.84 (dd, *J* = 2.9, 11.0 Hz, 1H), 4.11 (dd, *J* = 2.9, 7.6 Hz, 1H), 4.41 (q, *J* = 1.9 Hz, 1H), 4.72 (q, *J* = 1.9 Hz, 1H), 4.87 (d, *J* = 2.1 Hz, 2H), 5.00 (d, *J* = 4.8 Hz, 1H), 6.11 (d, *J* = 15.8 Hz, 1H), 6.73 (dd, *J* = 10.1, 15.9 Hz, 1H), 7.61 – 7.66 (m, 1H); **^{13}C NMR** (126 MHz, DMSO-d_6) δ 15.56, 23.13, 23.31, 27.79, 36.38, 38.16, 38.40, 42.50, 53.88, 60.72, 62.81, 70.28, 78.78, 108.16, 121.36, 127.27, 134.43, 146.83, 149.07, 172.51.

(3*E*,4*S*)-3-[2-[(4a*R*,6a*S*,7*R*,10b*R*)-3,3,6a,10b-Tetramethyl-8-methylene-1,4a,5,6,7,9,10, 10a-octahydronaphtho[2,1-*d*][1,3]dioxin-7-yl]ethylidene]-4-hydroxy-tetrahydrofuran-2-one (7)[13]

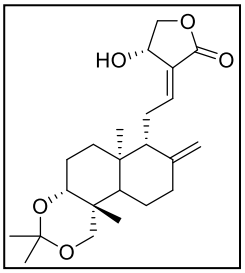

^{1}H NMR (500 MHz, DMSO-d_6) δ 0.87 (s, 3H), 1.13 (s, 3H), 1.15 – 1.35 (m, 3H), 1.29 (d, *J* = 39.6 Hz, 6H), 1.61 – 1.76 (m, 3H), 1.87 – 2.02 (m, 3H), 2.27 – 2.38 (m, 1H), 2.44 – 2.55 (m, 2H), 3.10 (d, *J* = 11.6 Hz, 1H), 3.40 (dd, *J* = 3.9, 9.1 Hz, 1H), 3.88 (d, *J* = 11.6 Hz, 1H), 4.03 (dd, *J* = 2.1, 9.9 Hz, 1H), 4.39 (dd, *J* = 6.1, 9.9 Hz, 1H), 4.60 – 4.90 (m, 2H), 4.88 – 4.95 (m, 1H), 5.69 (d, *J* = 6.1 Hz, 1H), 6.59 – 6.66 (m, 1H); **^{13}C NMR** (126 MHz, DMSO-d_6) δ 15.87, 22.86, 24.25, 25.03, 25.44, 25.97, 27.64, 34.20, 37.24, 37.33, 38.17, 51.69, 55.46, 62.94, 64.67, 74.45, 76.02, 98.30, 108.83, 129.19, 146.30, 147.68, 170.06.

[(3*R*,4*E*)-4-[2-[(4a*R*,6a*S*,7*R*,10b*R*)-3,3,6a,10b-Tetramethyl-8-methylene-1,4a,5,6,7,9,10, 10a-octahydronaphtho[2,1-*d*][1,3]dioxin-7-yl]ethylidene]-5-oxo-tetrahydrofuran-3-yl] acetate (8)[14]

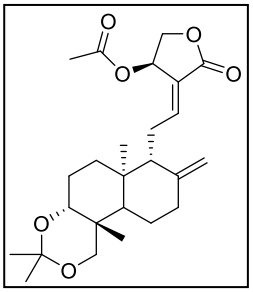

^{1}H NMR (500 MHz, DMSO-d_6) δ 0.87 (s, 3H), 1.13 (s, 3H), 1.20 – 1.35 (m, 10H), 1.62 – 1.76 (m, 3H), 1.87 – 1.96 (m, 2H), 1.93 – 2.02 (m, 1H), 2.30 – 2.38 (m, 1H), 2.46 – 2.54 (m, 2H), 3.10 (d, *J* = 11.5 Hz, 1H), 3.28 (s, 1H), 3.40 (dd, *J* = 3.9, 9.2 Hz, 1H), 3.88 (d, *J* = 11.6 Hz, 1H), 4.03 (dd, *J* = 2.1, 10.6 Hz, 1H), 4.39 (ddd, *J* = 1.0, 6.0, 9.9 Hz, 1H), 4.67 (s, 1H), 4.82 – 4.87 (m, 1H), 4.92 (t, *J* = 6.2 Hz, 1H), 5.69 (dd, *J* = 1.0, 6.0 Hz, 1H), 6.59 – 6.66 (m, 1H); **^{13}C NMR** (126 MHz, DMSO-d_6) δ 15.86, 22.85, 24.25, 25.03, 25.44, 25.97, 27.64, 34.20, 37.24, 37.33, 38.17, 51.69, 55.46, 62.94, 64.67, 74.44, 76.02, 98.29, 108.82, 129.18, 146.29, 147.68, 170.05.

14β-Andrographolide (9)[14]

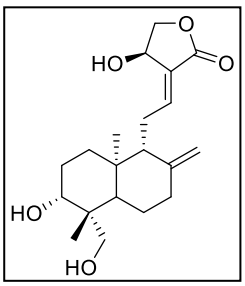

^{1}H NMR (600 MHz, DMSO-d_6) δ 0.65 (s, 3H), 1.08 (s, 3H), 1.16 – 1.24 (m, 2H), 1.29 – 1.39 (m, 1H), 1.59 – 1.77 (m, 4H), 1.85 (dd, *J* = 3.3, 11.1 Hz, 1H), 1.88 – 1.97 (m, 1H), 2.28 – 2.34 (m, 1H), 2.40 – 2.54 (m, 2H), 3.19 – 3.28 (m, 2H), 3.83 (dd, *J* = 2.9, 11.0 Hz, 1H), 4.02 (dd, *J* = 2.1, 9.9 Hz, 1H), 4.11 (dd, *J* = 2.9, 7.5 Hz, 1H), 4.38 (dd, *J* = 6.1, 9.9 Hz, 1H), 4.62 (d, *J* = 1.7 Hz, 1H), 4.81 (d, *J* = 1.7 Hz, 1H), 4.90 (t, *J* = 6.0 Hz, 1H), 5.02 (d, *J* = 4.9 Hz, 1H), 5.68 (d, *J* = 6.1 Hz, 1H), 6.61 (td, *J* = 1.8, 6.8 Hz, 1H); **^{13}C NMR** (151 MHz, DMSO-d_6) δ 14.89, 23.21, 24.10, 28.04, 36.67, 37.65, 38.73, 39.28, 39.42, 39.56, 42.43, 54.53, 55.64, 62.78, 64.67, 74.45, 78.59, 108.36, 129.12, 146.40, 147.75, 170.07.

(4*S*)-3-[2-[(4a*R*,6a*S*,7*R*,10b*R*)-3,3,6a,10b-Tetramethyl-8-methylene-1,4a,5,6,7,9,10,10a-octahydronaphtho[2,1-*d*][1,3]dioxin-7-yl]ethyl]-4-hydroxy-tetrahydrofuran-2-one (10)[15]

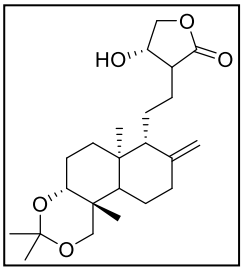

^{1}H NMR (600 MHz, DMSO-d_6) δ 0.82 (s, 3H), 1.11 (s, 3H), 1.15 – 1.40 (m, 10H), 1.41 – 1.53 (m, 2H), 1.54 – 1.74 (m, 5H), 1.85 – 1.96 (m, 2H), 2.29 – 2.36 (m, 1H), 2.54 – 2.60 (m, 1H), 3.08 (d, *J* = 11.6 Hz, 1H), 3.39 (dd, *J* = 4.0, 9.0 Hz, 1H), 3.85 (d, *J* = 11.6 Hz, 1H), 4.04 (d, *J* = 9.7 Hz, 1H), 4.23 (dd, *J* = 3.2, 9.8 Hz, 1H), 4.36 (td, *J* = 3.3, 4.9 Hz, 1H), 4.68 (d, *J* = 1.7 Hz, 1H), 4.81 (d, *J* = 1.8 Hz, 1H), 5.37 (d, *J* = 4.4 Hz, 1H); **^{13}C NMR** (151 MHz, DMSO-d_6) δ 16.12, 21.57, 22.63, 23.08, 24.92, 25.37, 25.94, 27.48, 34.16, 37.42, 37.69, 38.28, 39.28, 44.67, 51.70, 55.63, 63.04, 67.76, 74.79, 75.88, 98.34, 107.56, 147.68, 178.50.

(4*S*)-3-[2-[(1*R*,5*R*,6*R*,8a*S*)-6-Hydroxy-5-(hydroxymethyl)-5,8a-dimethyl-2-methylene-decalin-1-yl]ethyl]-4-hydroxy-tetrahydrofuran-2-one (11)[15]

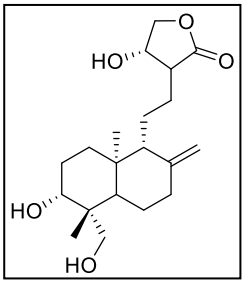

^{1}H NMR (600 MHz, DMSO-d_6) δ 0.65 (s, 3H), 1.08 (s, 3H), 1.16 – 1.24 (m, 2H), 1.29 – 1.39 (m, 1H), 1.59 – 1.77 (m, 4H), 1.85 (dd, *J* = 3.3, 11.1 Hz, 1H), 1.88 – 1.97 (m, 1H), 2.28 – 2.34 (m, 1H), 2.40 – 2.54 (m, 2H), 3.19 – 3.28 (m, 2H), 3.83 (dd, *J* = 2.9, 11.0 Hz, 1H), 4.02 (dd, *J* = 2.1, 9.9 Hz, 1H), 4.11 (dd, *J* = 2.9, 7.5 Hz, 1H), 4.38 (dd, *J* = 6.1, 9.9 Hz, 1H), 4.62 (d, *J* = 1.7 Hz, 1H), 4.81 (d, *J* = 1.7 Hz, 1H), 4.90 (t, *J* = 6.0 Hz, 1H), 5.02 (d, *J* = 4.9 Hz, 1H), 5.68 (d, *J* = 6.1 Hz, 1H), 6.61 (td, *J* = 1.8, 6.8 Hz, 1H); **^{13}C NMR** (151 MHz, DMSO-d_6) δ 14.89, 23.21, 24.10, 28.04, 36.67, 37.65, 38.73, 39.28, 39.42, 39.56, 42.43, 54.53, 55.64, 62.78, 64.67, 74.45, 78.59, 108.36, 129.12, 146.40, 147.75, 170.07.

(3*E*,4*S*)-3-[2-[(1*R*,5*R*,6*R*,8a*S*)-6-Hydroxy-5-(hydroxymethyl)-5,8a-dimethyl-2-methylene-decalin-1-yl]ethylidene]-4-[*tert*-butyl(dimethyl)silyl]oxy-tetrahydrofuran-2-one (12)[16]

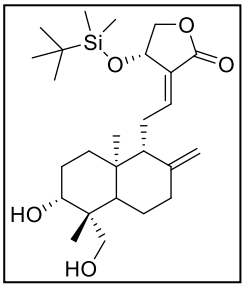

^{1}H NMR (500 MHz, DMSO-d_6) δ 0.11 (s, 3H), 0.14 (s, 3H), 0.86 (s, 9H), 1.08 (s, 3H), 1.17 – 1.26 (m, 2H), 1.27 – 1.39 (m, 1H), 1.58 – 1.76 (m, 4H), 1.91 – 1.99 (m, 2H), 2.27 – 2.35 (m, 1H), 2.40 – 2.47 (m, 2H), 3.18 – 3.27 (m, 2H), 3.79 – 3.86 (m, 1H), 3.99 (dd, *J* = 2.3, 10.0 Hz, 1H), 4.06 – 4.12 (m, 1H), 4.45 (dd, *J* = 5.9, 10.0 Hz, 1H), 4.47 – 4.81 (m, 2H), 4.99 – 5.04 (m, 1H), 5.15 – 5.21 (m, 1H), 6.56 – 6.63 (m, 1H); **^{13}C NMR** (126 MHz, DMSO-d_6) δ -4.83, -4.34, 15.00, 17.60, 23.21, 24.00, 24.39, 25.69, 27.98, 36.87, 37.52, 38.58, 42.41, 54.45, 55.44, 62.74, 66.55, 74.02, 78.55, 108.53, 127.77, 147.49, 147.96, 169.53.

(1*S*,2*R*,4a*S*,5*R*)-5-[(2*E*)-2-[(4*S*)-4-[*tert*-Butyl(dimethyl)silyl]oxy-2-oxo-tetrahydrofuran-3-ylidene]ethyl]-2-hydroxy-1,4a-dimethyl-6-methylene-decalin-1-carbaldehyde (13)[16]

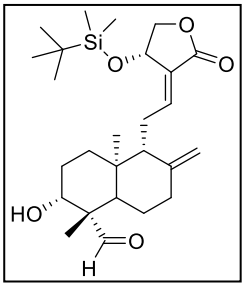

^{1}H NMR (500 MHz, DMSO-d_6) δ 0.11 (s, 3H), 0.14 (s, 3H), 0.55 (s, 3H), 0.85 (s, 9H), 1.08 (s, 3H), 1.04 – 1.19 (m, 4H), 1.30 – 1.41 (m, 1H), 1.39 – 1.48 (m, 1H), 1.72 – 1.87 (m, 3H), 1.91 – 2.01 (m, 2H), 2.01 – 2.06 (m, 1H), 2.25 – 2.34 (m, 1H), 2.39 – 2.55 (m, 2H), 3.30 – 3.39 (m, 1H), 4.00 (dd, *J* = 2.4, 9.9 Hz, 1H), 4.46 (dd, *J* = 5.9, 10.0 Hz, 1H), 4.51 (d, *J* = 1.7 Hz, 1H), 4.80 (d, *J* = 1.9 Hz, 1H), 5.11 (d, *J* = 4.5 Hz, 1H), 5.17 – 5.23 (m, 1H), 6.57 – 6.64 (m, 1H), 9.95 (s, 1H); **^{13}C NMR** (126 MHz, DMSO-d_6) δ –4.84, –4.35, 15.18, 17.59, 21.09, 23.89, 24.59, 25.68, 28.06, 36.10, 36.87, 38.63, 52.94, 53.88, 54.95, 66.56, 74.00, 75.05, 108.99, 127.78, 147.32, 147.54, 169.49, 207.29.

(1*S*,2*R*,4a*S*,5*R*)-5-[(2*E*)-2-[(4*S*)-4-[*tert*-Butyl(dimethyl)silyl]oxy-2-oxo-tetrahydrofuran-3-ylidene]ethyl]-2-hydroxy-1,4a-dimethyl-6-methylene-decalin-1-carboxylic acid (14)[16]

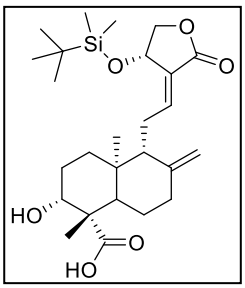

^{1}H NMR (500 MHz, DMSO-d_6) δ 0.11 (s, 3H), 0.14 (s, 3H), 0.64 (s, 3H), 0.86 (s, 9H), 1.27 (s, 3H), 1.22 – 1.35 (m, 2H), 1.53 – 1.67 (m, 2H), 1.68 – 1.76 (m, 1H), 1.85 – 1.92 (m, 1H), 1.92 – 2.01 (m, 2H), 2.03 – 2.15 (m, 1H), 2.29 – 2.37 (m, 1H), 2.43 – 2.51 (m, 2H), 3.10 (dd, *J* = 4.4, 12.0 Hz, 1H), 4.00 (dd, *J* = 2.3, 9.9 Hz, 1H), 4.36 (s, 1H), 4.46 (dd, *J* = 6.0, 9.9 Hz, 1H), 4.51 (s, 1H), 4.82 (s, 1H), 5.19 (d, *J* = 5.8 Hz, 1H), 6.60 (td, *J* = 1.7, 6.5 Hz, 1H), 12.28 (s, 1H); **^{13}C NMR** (126 MHz, DMSO-d_6) δ –4.87, –4.35, 12.93, 17.59, 24.36, 24.39, 25.25, 25.67, 28.41, 37.20, 37.38, 48.91, 53.97, 54.88, 66.56, 73.99, 76.67, 108.67, 127.75, 128.01, 147.45, 147.80, 169.50, 177.25.

(1*S*,2*R*,4a*S*,5*R*)-2-Hydroxy-5-[(2*E*)-2-[(4*S*)-4-hydroxy-2-oxo-tetrahydrofuran-3-ylidene]ethyl]-1,4a-dimethyl-6-methylene-decalin-1-carboxylic acid (15)

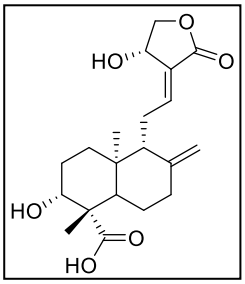

^{1}H NMR (500 MHz, DMSO-d_6) δ 0.65 (s, 3H), 1.20 – 1.33 (m, 6H), 1.56 – 1.69 (m, 2H), 1.74 – 1.81 (m, 1H), 1.83 – 1.98 (m, 3H), 2.03 – 2.15 (m, 1H), 2.30 – 2.37 (m, 1H), 2.41 – 2.50 (m, 1H), 2.50 – 2.59 (m, 1H), 3.09 (dd, *J* = 4.4, 12.0 Hz, 1H), 4.03 (dd, *J* = 2.1, 9.9 Hz, 1H), 4.39 (dd, *J* = 6.1, 10.0 Hz, 1H), 4.63 (s, 1H), 4.84 (d, *J* = 1.6 Hz, 1H), 4.91 (d, *J* = 6.0 Hz, 1H), 5.68 (s, 1H), 6.62 (td, *J* = 1.8, 6.8 Hz, 1H), 12.24 (s, 1H); **^{13}C NMR** (126 MHz, DMSO-d_6) δ 12.77, 24.09, 24.36, 25.35, 28.48, 37.03, 37.53, 48.93, 54.10, 55.12, 64.67, 74.44, 76.73, 108.47, 129.14, 146.35, 147.60, 170.05, 177.30.

(1*S*,2*R*,4a*S*,5*R*)-2-Hydroxy-5-[(2*E*)-2-[(4S)-4-hydroxy-2-oxo-tetrahydrofuran-3-ylidene]ethyl]-1,4a-dimethyl-6-methylene-*N*-propyl-decalin-1-carboxamide (16a)

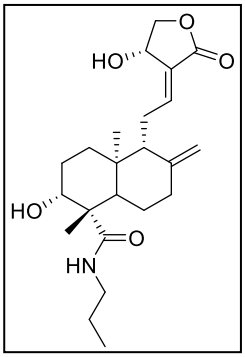

^{1}H NMR (600 MHz, DMSO-d_6) δ 0.58 (s, 3H), 0.83 (t, *J* = 7.4 Hz, 3H), 1.14 – 1.22 (m, 1H), 1.20 (s, 3H), 1.22 – 1.30 (m, 1H), 1.32 – 1.42 (m, 2H), 1.61 – 1.68 (m, 1H), 1.73 – 1.79 (m, 1H), 1.82 – 2.01 (m, 4H), 2.06 – 2.17 (m, 1H), 2.28 – 2.34 (m, 1H), 2.40 – 2.56 (m, 2H), 2.92 – 3.06 (m, 2H), 3.18 – 3.25 (m, 1H), 4.02 (dd, *J* = 2.1, 9.9 Hz, 1H), 4.38 (dd, *J* = 6.1, 9.9 Hz, 1H), 4.60 (s, 1H), 4.82 (s, 1H), 4.87 – 4.93 (m, 1H), 5.56 (d, *J* = 5.1 Hz, 1H), 5.68 (d, *J* = 6.1 Hz, 1H), 6.62 (td, *J* = 1.8, 6.9 Hz, 1H), 7.83 (t, *J* = 5.6 Hz, 1H); **^{13}C NMR** (151 MHz, DMSO-d_6) δ 11.64, 13.48, 22.32, 24.15, 24.88, 25.82, 28.76, 37.56, 38.14, 48.23, 55.15, 55.36, 64.66, 74.45, 76.95, 107.96, 129.10, 146.51, 147.96, 170.08, 175.23.

(1*S*,2*R*,4a*S*,5*R*)-2-Hydroxy-5-[(2*E*)-2-[(4*S*)-4-hydroxy-2-oxo-tetrahydrofuran-3-ylidene]ethyl]-1,4a-dimethyl-6-methylene-*N*-(2-phenylethyl)decalin-1-carboxamide (16b)

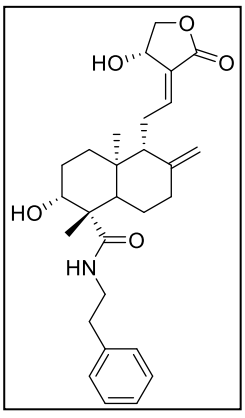

^{1}H NMR (500 MHz, DMSO-d_6) δ 0.53 (s, 3H), 1.06 – 1.31 (m, 5H), 1.51 – 1.60 (m, 1H), 1.66 – 1.77 (m, 1H), 1.79 – 1.92 (m, 4H), 2.03 – 2.16 (m, 1H), 2.26 – 2.34 (m, 1H), 2.38 – 2.56 (m, 2H), 2.68 (t, *J* = 7.1 Hz, 2H), 3.13 – 3.21 (m, 1H), 3.22 – 3.38 (m, 2H), 4.03 (dd, *J* = 2.0, 9.9 Hz, 1H), 4.38 (dd, *J* = 6.1, 9.9 Hz, 1H), 4.59 (s, 1H), 4.82 (d, *J* = 1.8 Hz, 1H), 4.89 (tt, *J* = 1.9, 6.0 Hz, 1H), 5.48 (d, *J* = 4.9 Hz, 1H), 5.67 (d, *J* = 6.1 Hz, 1H), 6.61 (td, *J* = 1.7, 6.7 Hz, 1H), 7.14 – 7.22 (m, 3H), 7.22 – 7.30 (m, 2H), 7.85 (t, *J* = 5.6 Hz, 1H); **^{13}C NMR** (126 MHz, DMSO-d_6) δ 13.51, 24.10, 24.85, 25.76, 28.60, 35.13, 37.54, 38.12, 40.12, 40.20, 40.29, 48.21, 55.15, 55.35, 64.65, 74.43, 76.87, 107.92, 126.17, 128.39, 128.73, 129.09, 139.64, 146.49, 147.92, 170.07, 175.30.

(1*S*,2*R*,4a*S*,5*R*)-2-Hydroxy-5-[(2*E*)-2-[(4*S*)-4-hydroxy-2-oxo-tetrahydrofuran-3-ylidene]ethyl]-N-[2-[2-[2-(2-methoxyethoxy)ethoxy]ethoxy]ethyl]-1,4a-dimethyl-6-methylene-decalin-1-carboxamide (16c)

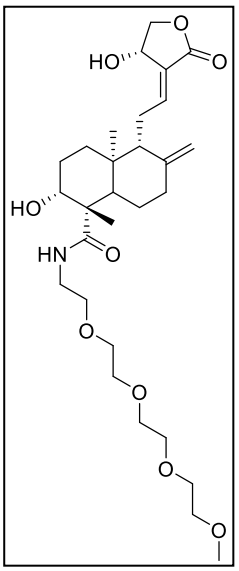

^{1}H NMR (600 MHz, DMSO-d_6) δ 0.58 (s, 3H), 1.20 (s, 3H), 1.21 – 1.30 (m, 2H), 1.59 – 1.67 (m, 1H), 1.71 – 1.80 (m, 1H), 1.81 – 2.03 (m, 4H), 2.07 – 2.18 (m, 1H), 2.28 – 2.34 (m, 1H), 2.40 – 2.48 (m, 1H), 2.54 (s, 1H), 3.09 – 3.17 (m, 1H), 3.17 – 3.29 (m, 5H), 3.34 – 3.44 (m, 4H), 3.44 – 3.52 (m, 10H), 4.00 – 4.05 (m, 1H), 4.34 – 4.41 (m, 1H), 4.60 (s, 1H), 4.82 (s, 1H), 4.87 – 4.93 (m, 1H), 5.50 – 5.54 (m, 1H), 5.66 – 5.71 (m, 1H), 6.58 – 6.64 (m, 1H), 7.91 – 7.96 (m, 1H); **^{13}C NMR** (151 MHz, DMSO-d_6) δ 13.46, 24.16, 24.80, 25.80, 28.65, 37.56, 38.17, 38.30, 40.12, 48.25, 55.18, 55.41, 58.22, 64.69, 69.16, 69.70 – 70.10 (m), 71.45, 74.49, 76.89, 107.96, 129.13, 146.57, 146.58, 148.00, 170.14, 175.38.

NMR and HRMS Spectra

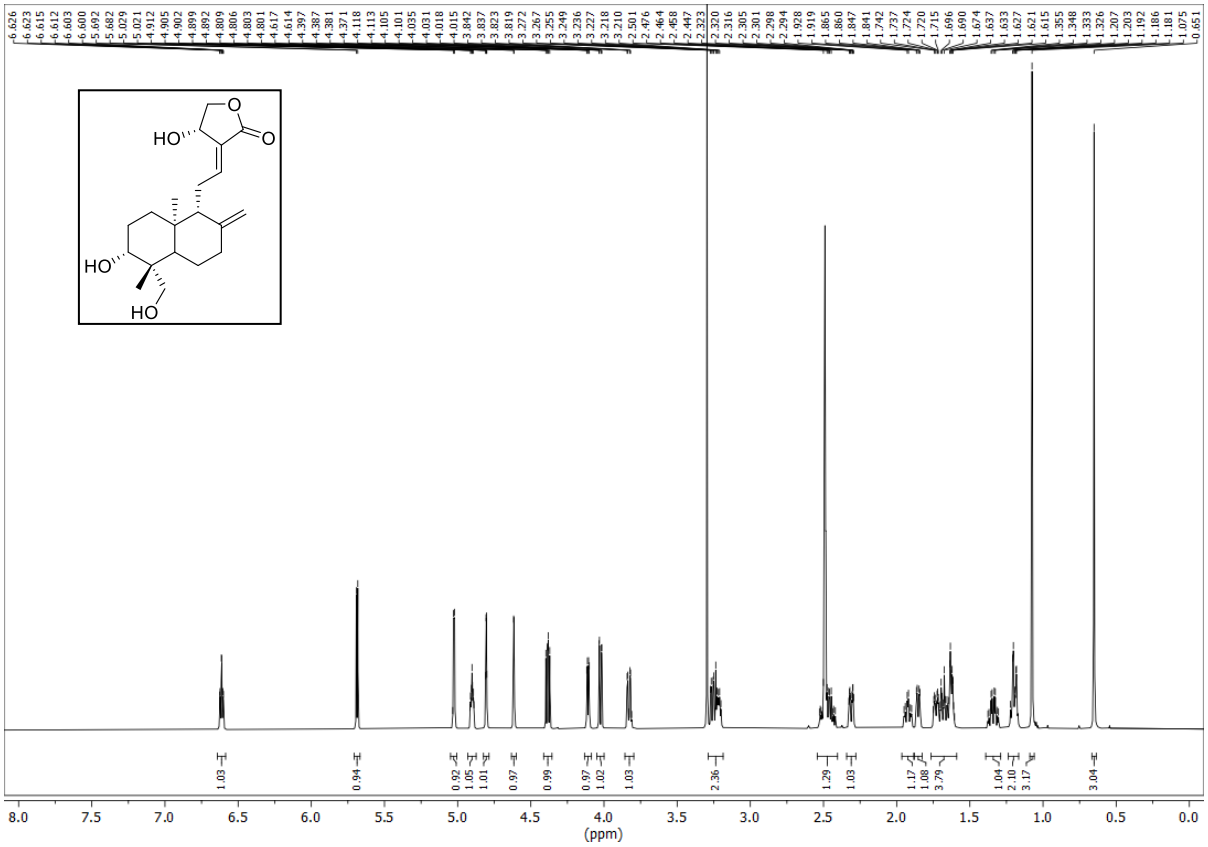

^{1}H NMR spectrum of **1**.

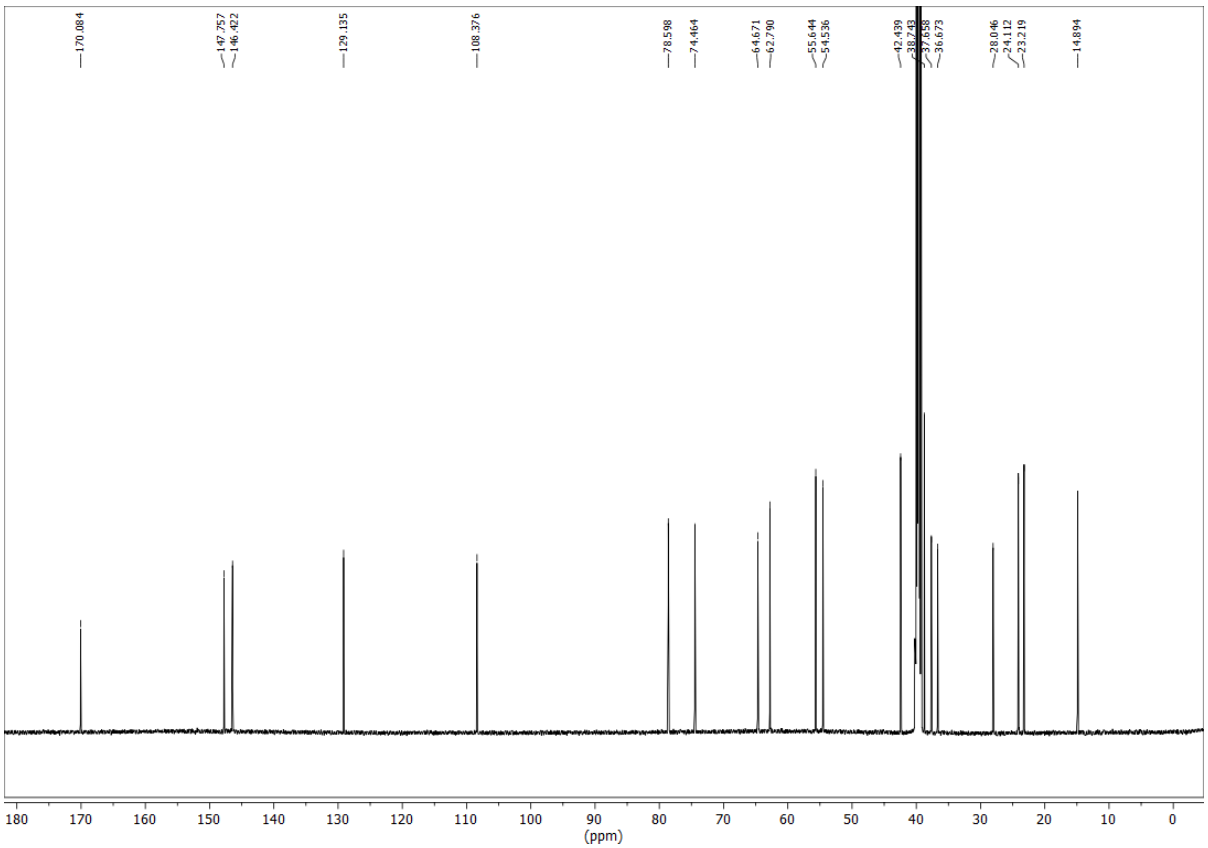

^{13}C NMR spectrum of **1**.

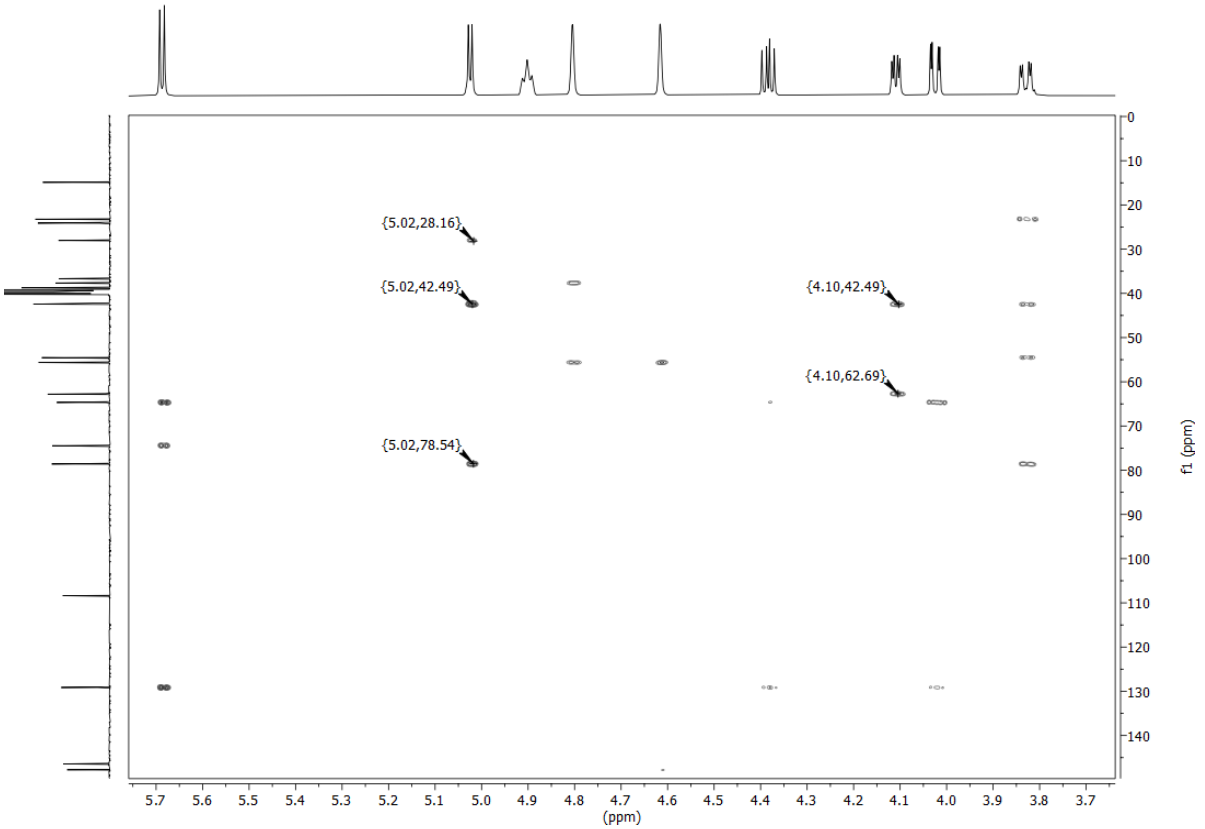

^{1}H-HMBC NMR spectrum of **1**.

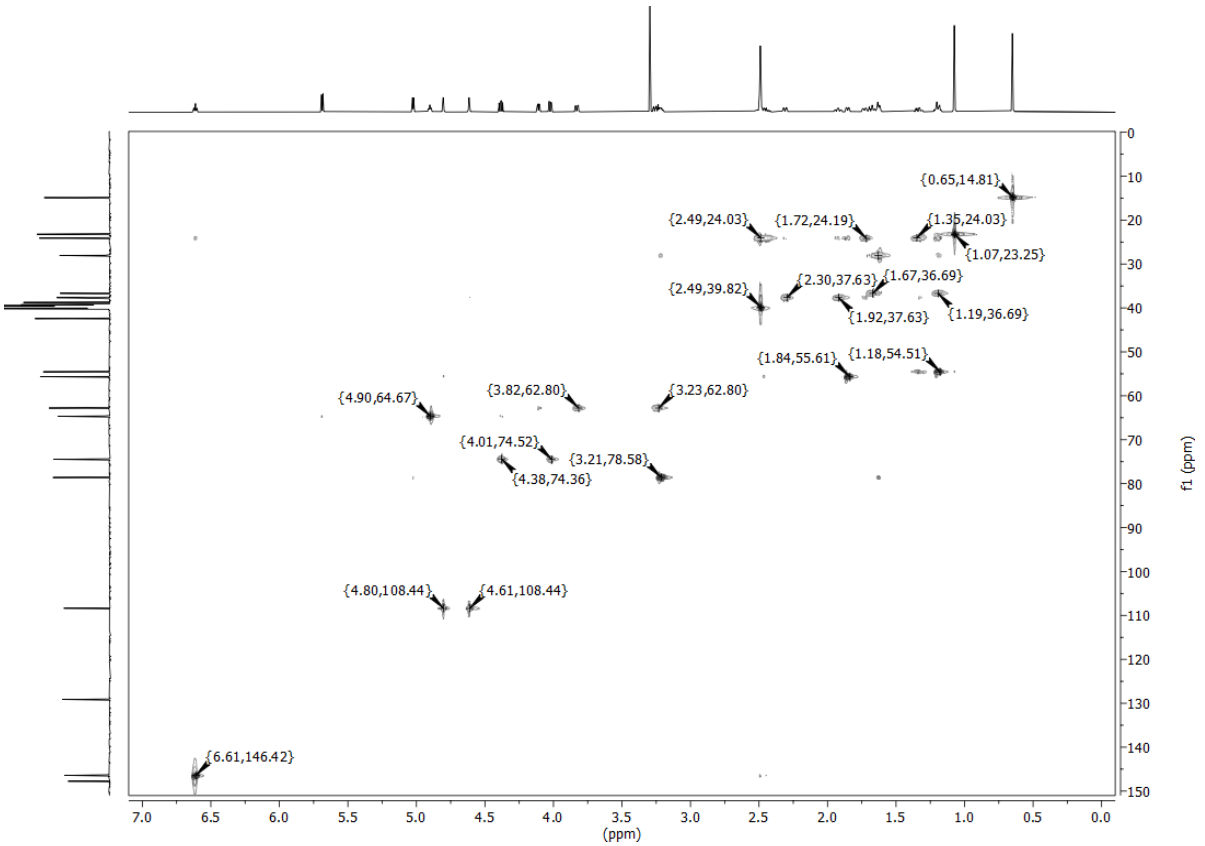

^{1}H,^{13}C-HSQC NMR spectrum of **1**.

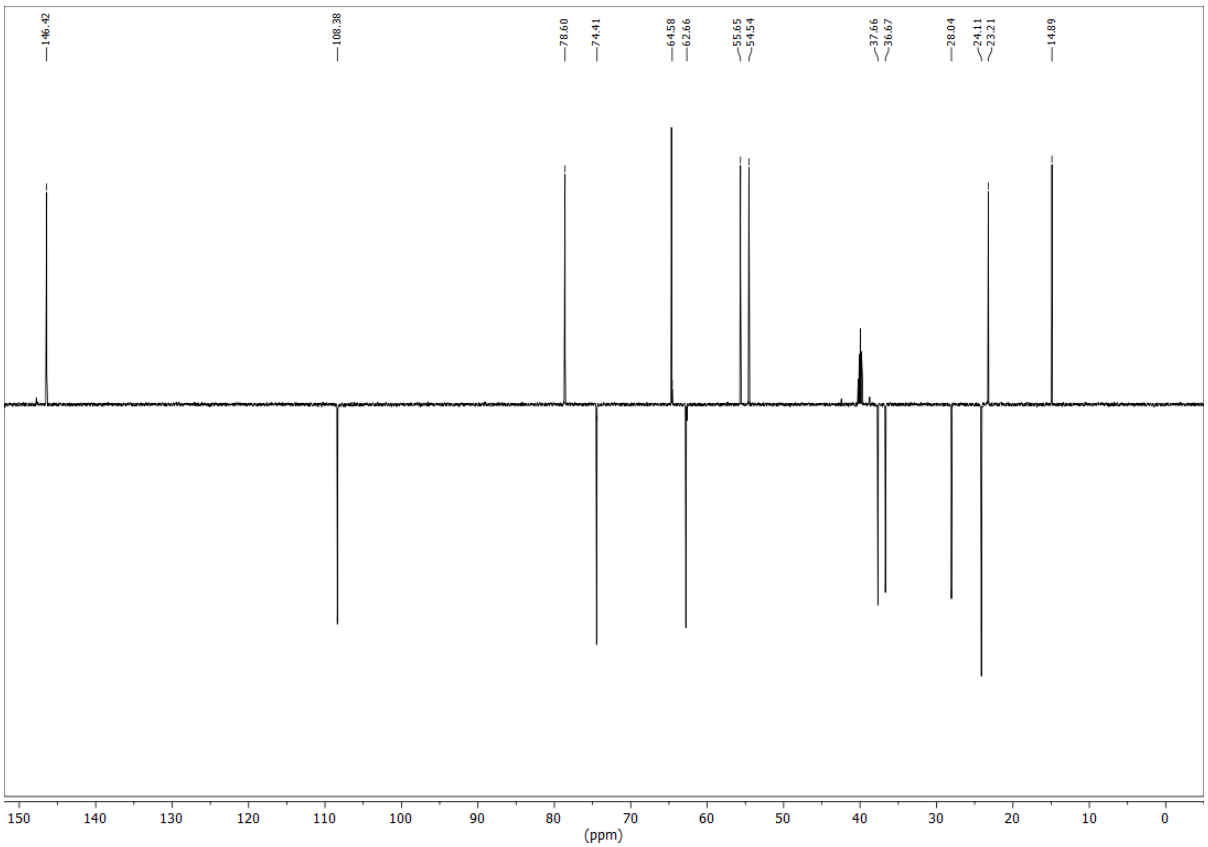

DEPT-135 NMR spectrum of **1**.

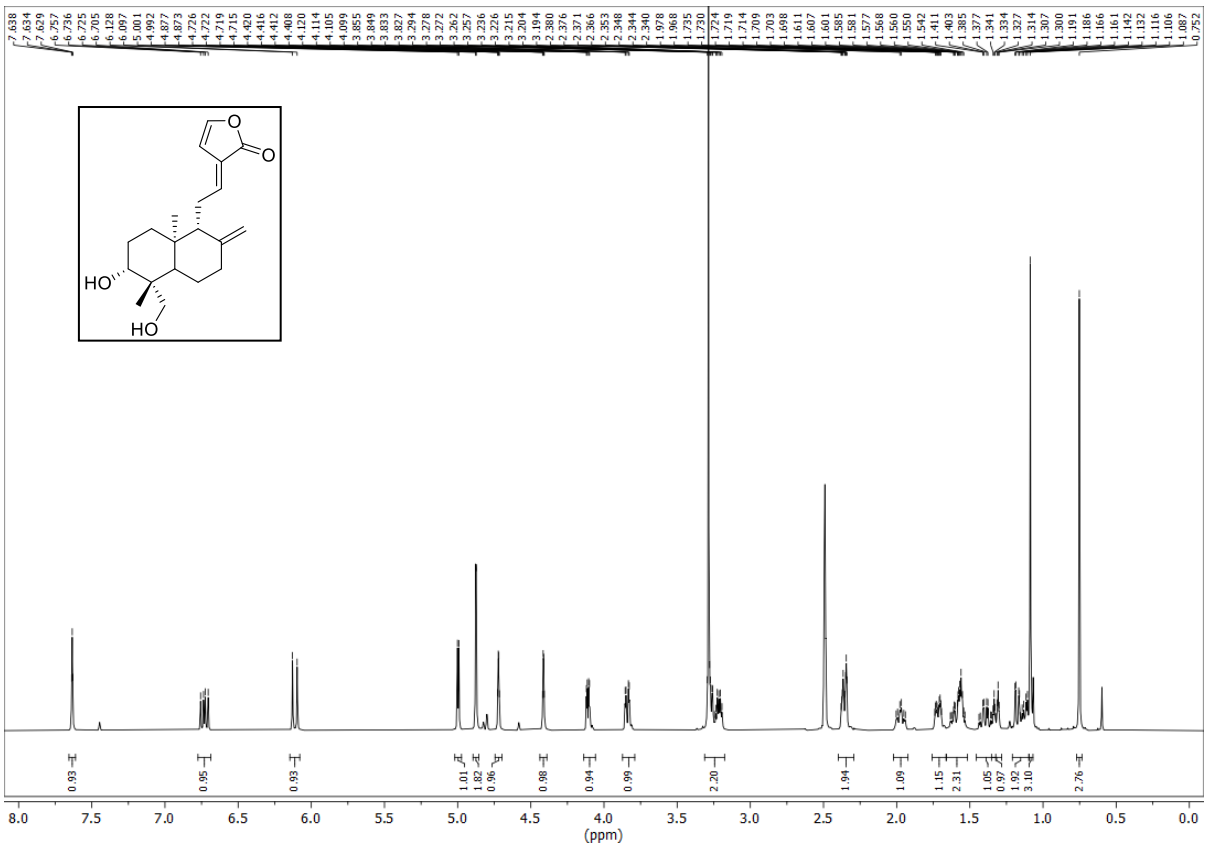

^{1}H NMR spectrum of **2**.

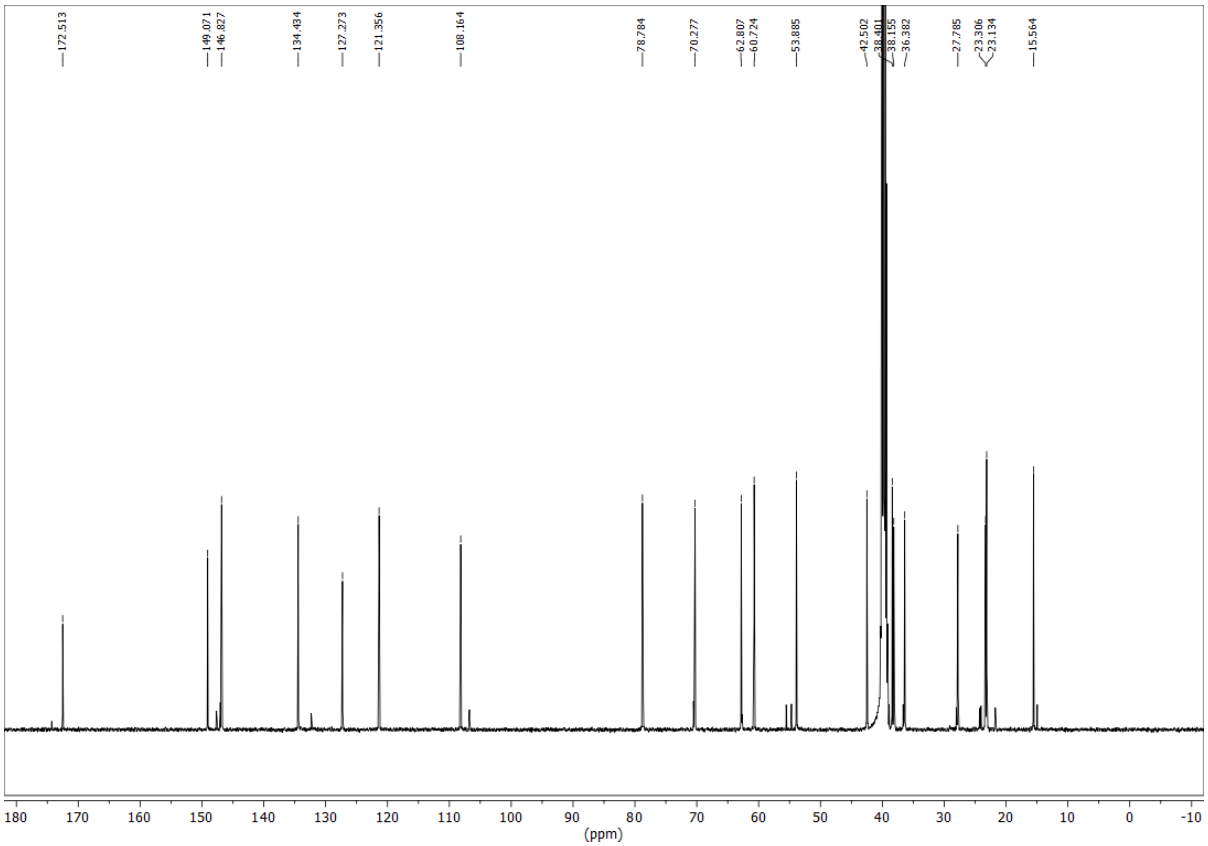

^{13}C NMR spectrum of **2**.

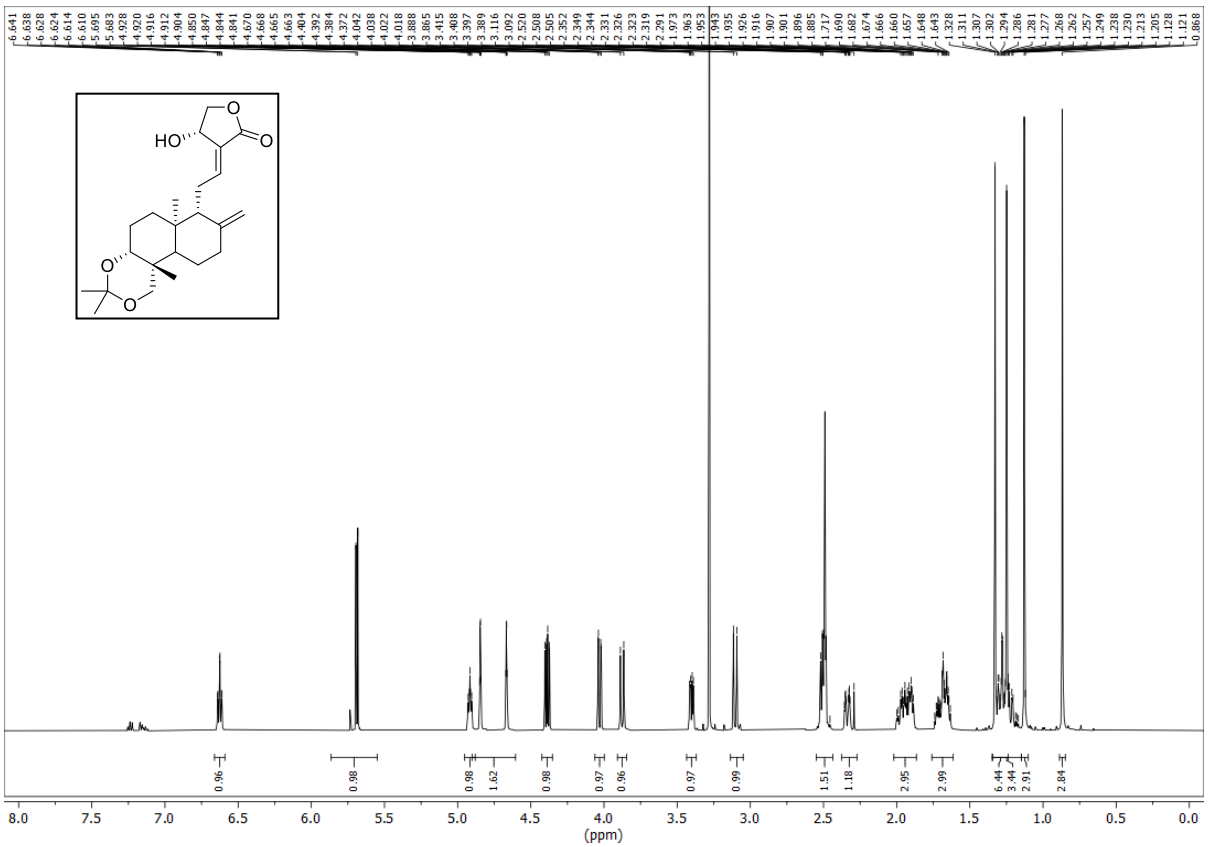

^{1}H NMR spectrum of **7**.

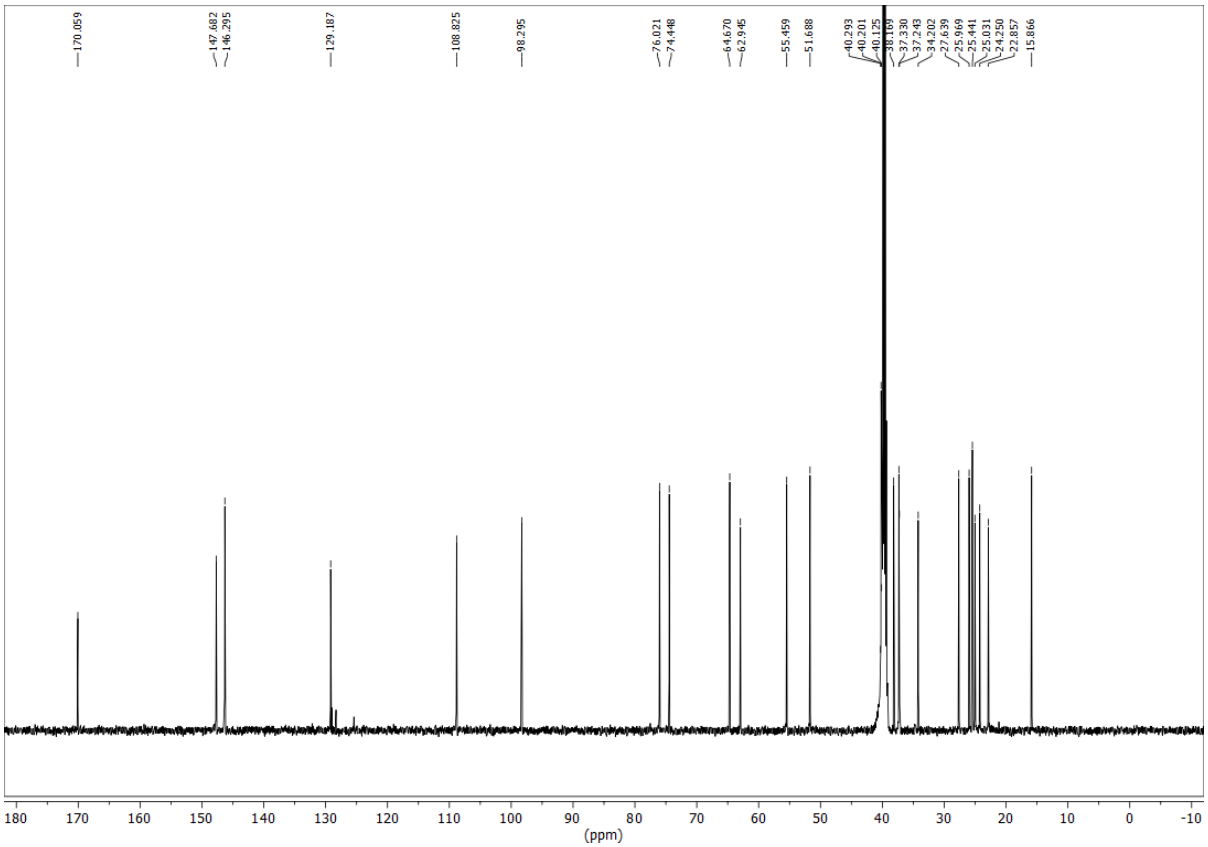

^{13}C NMR spectrum of **7**.

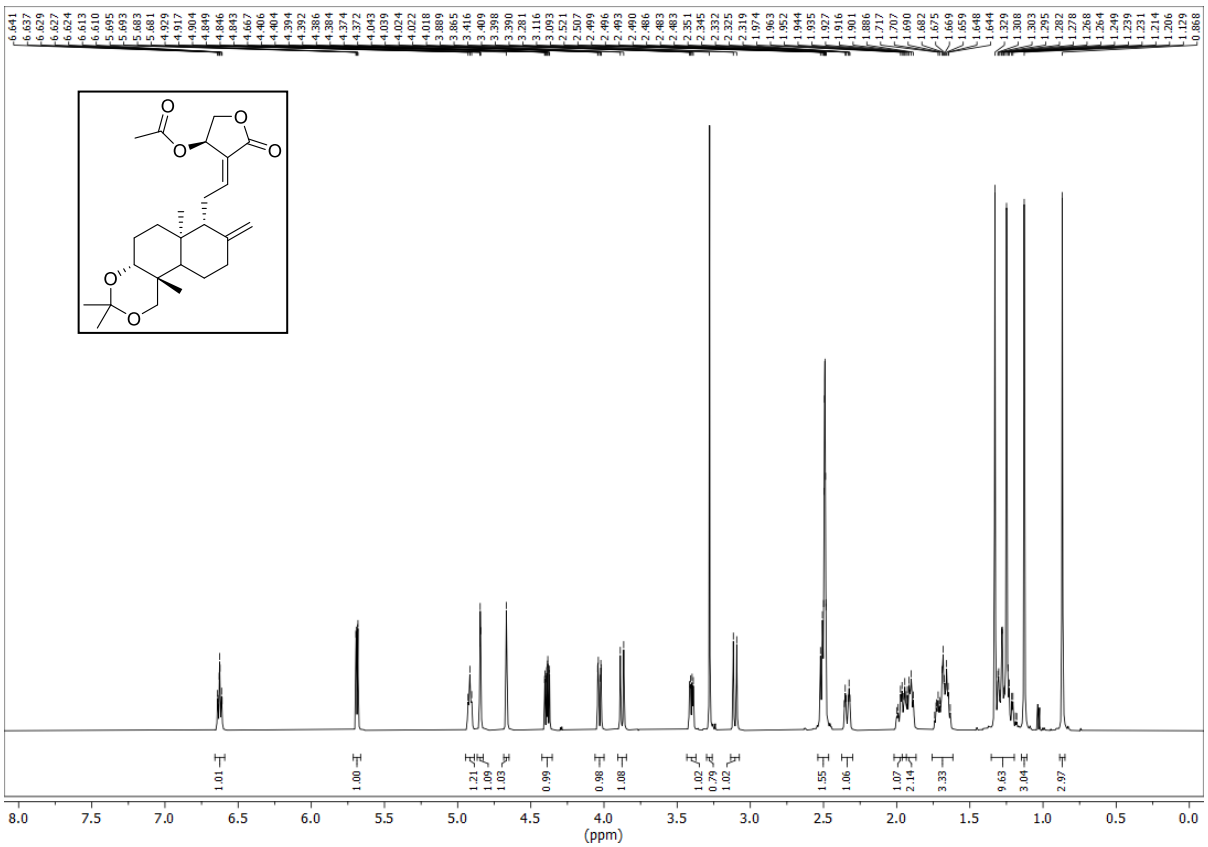

^{1}H NMR spectrum of **8**.

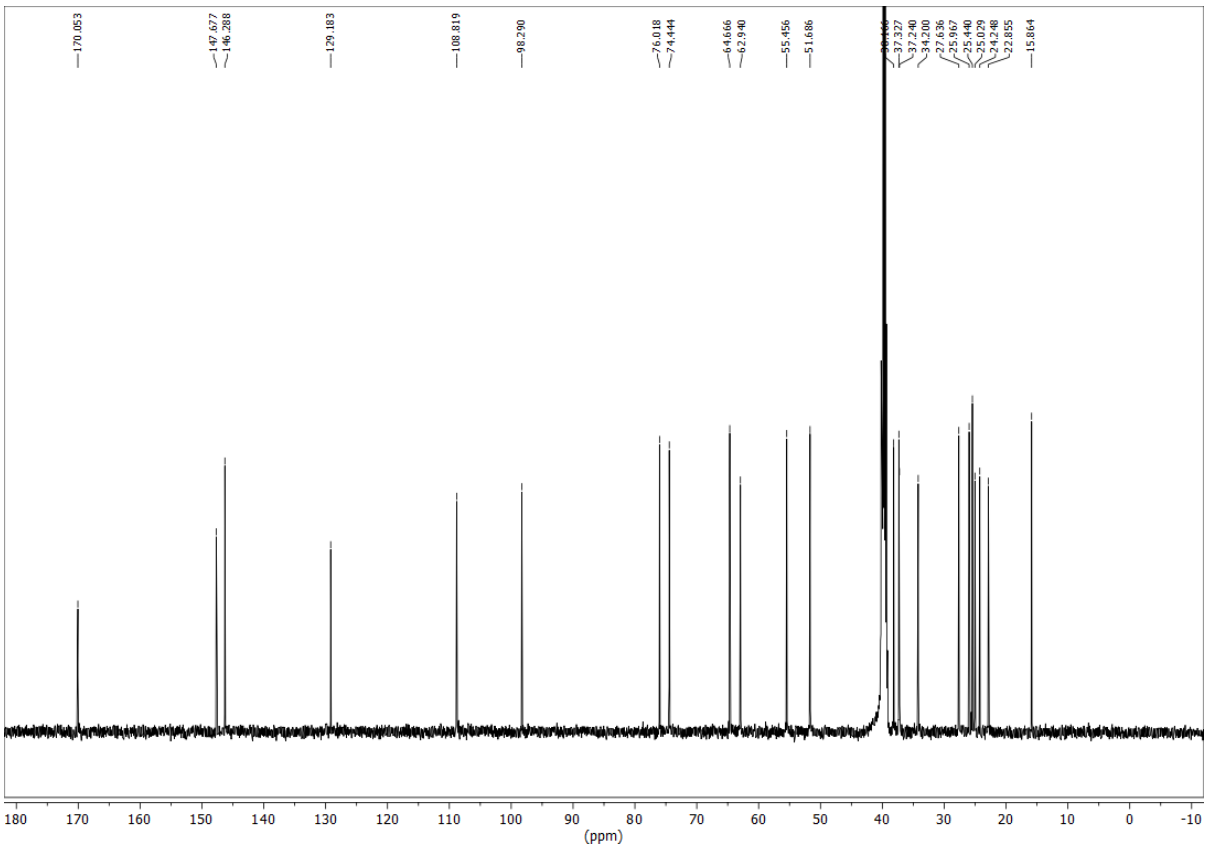

^{13}C NMR spectrum of **8**.

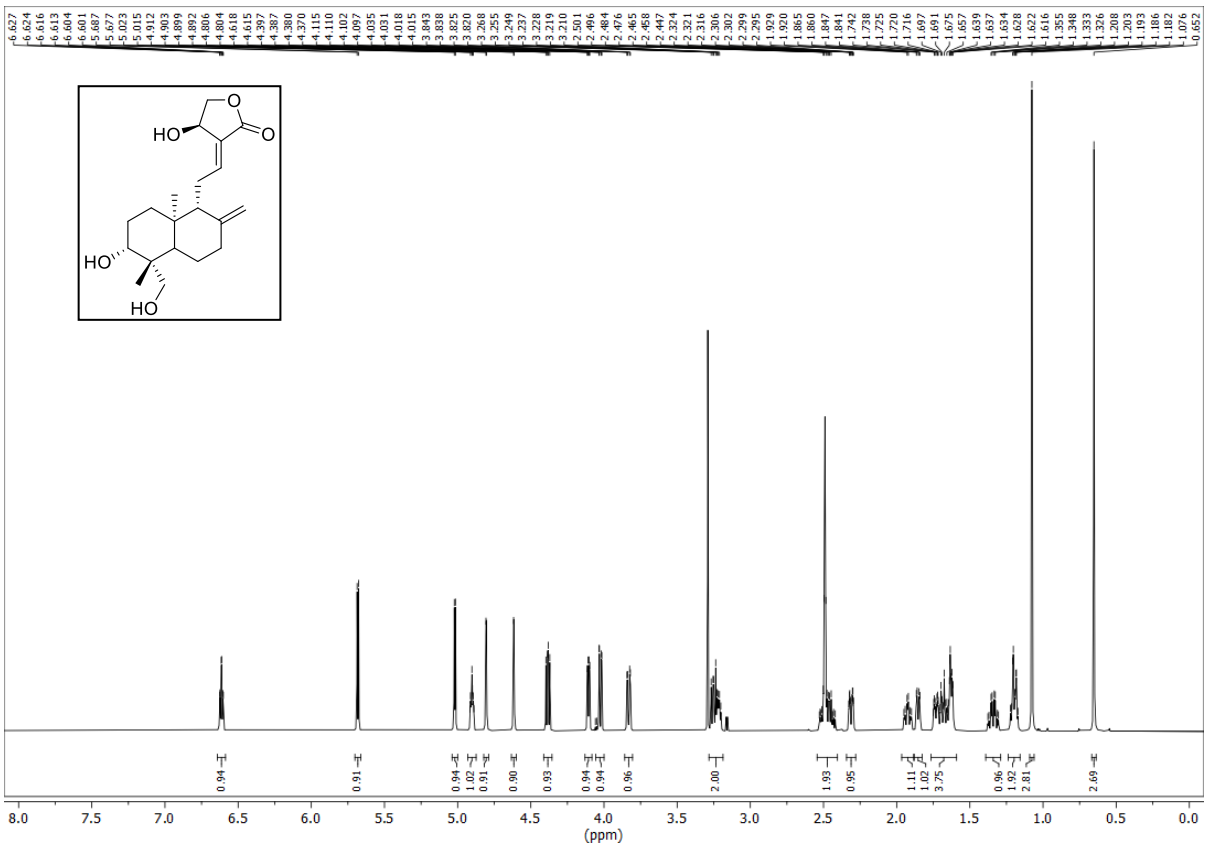

^{1}H NMR spectrum of **9**.

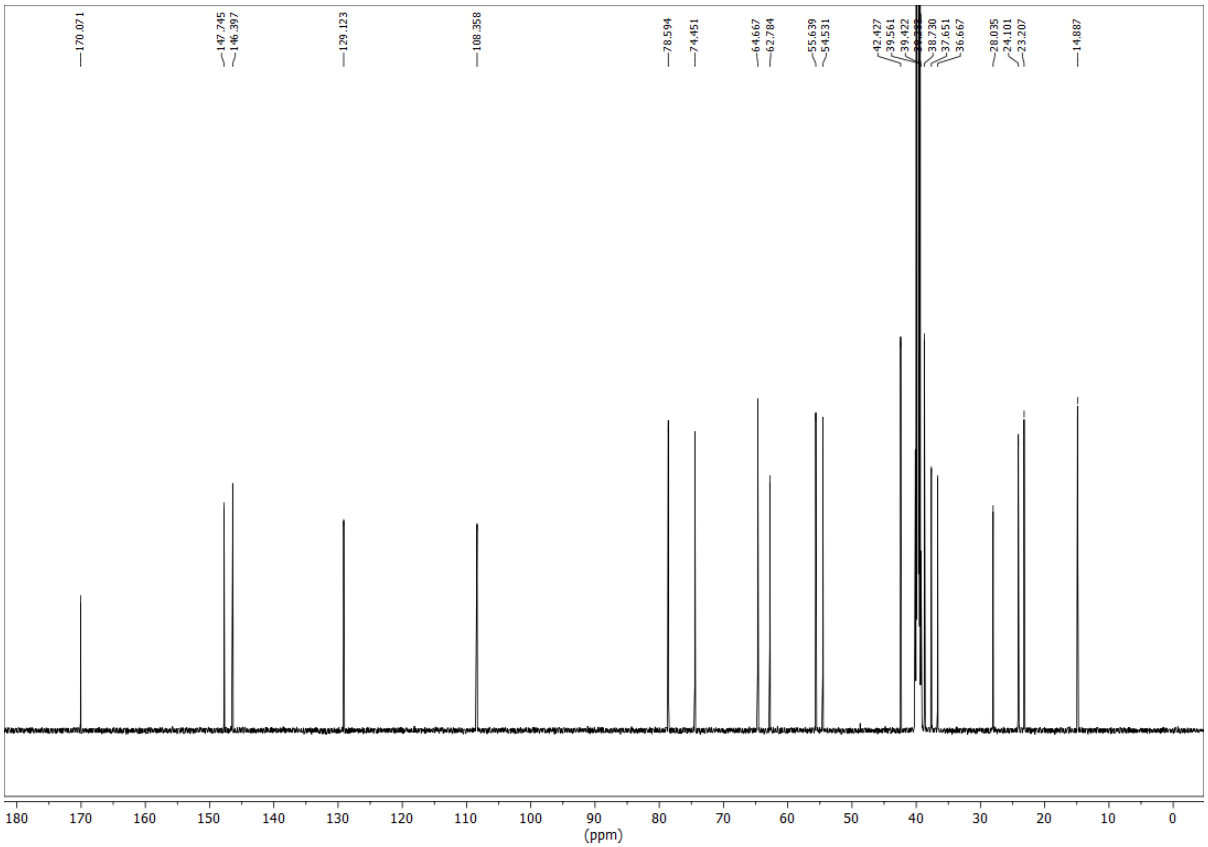

^{13}C NMR spectrum of **9**.

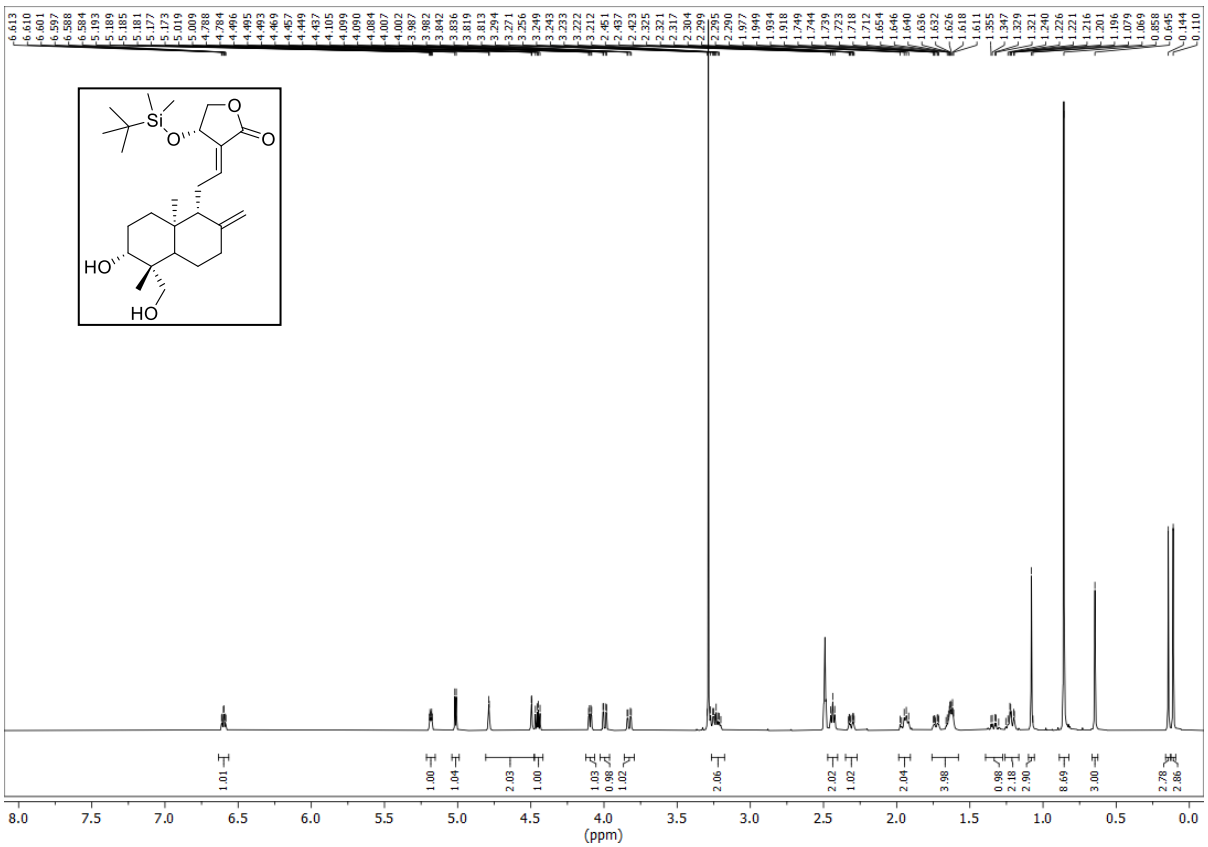

^{1}H NMR spectrum of **12**.

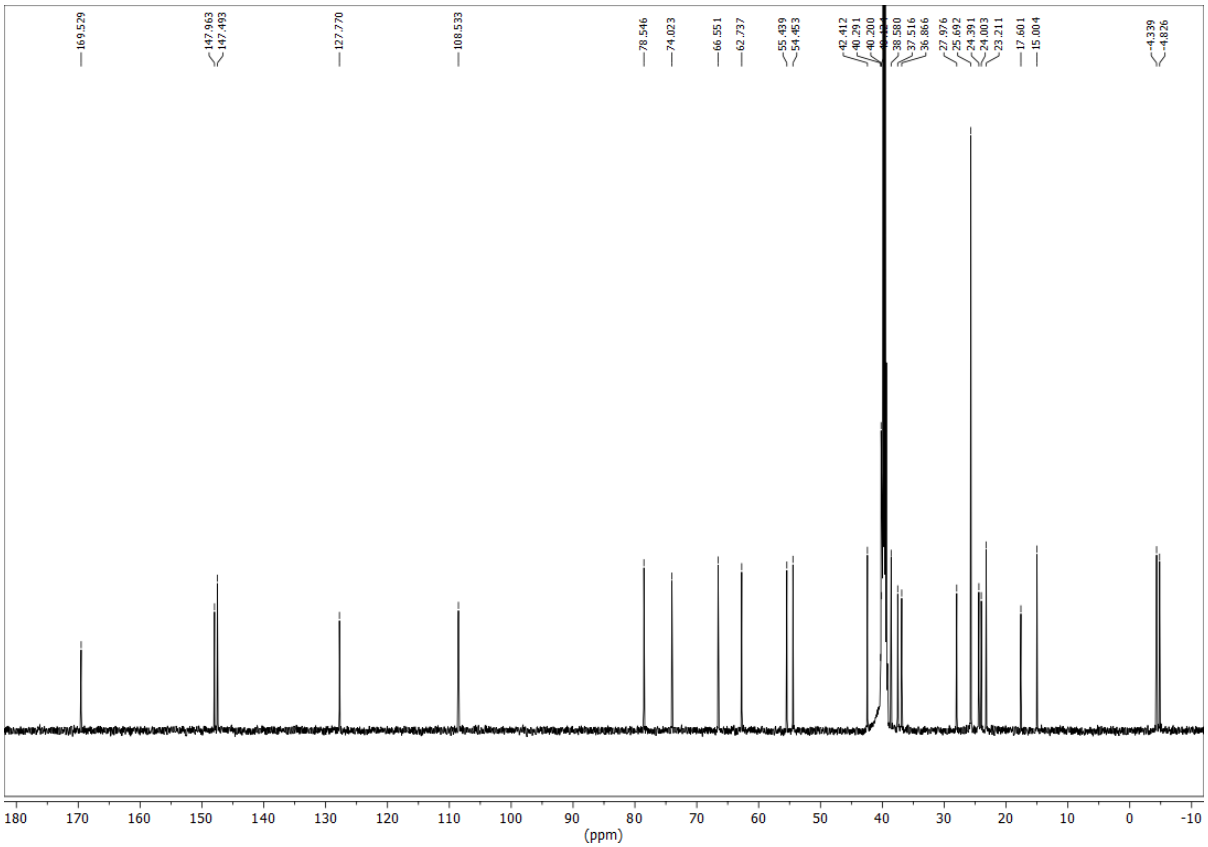

^{13}C NMR spectrum of **12**.

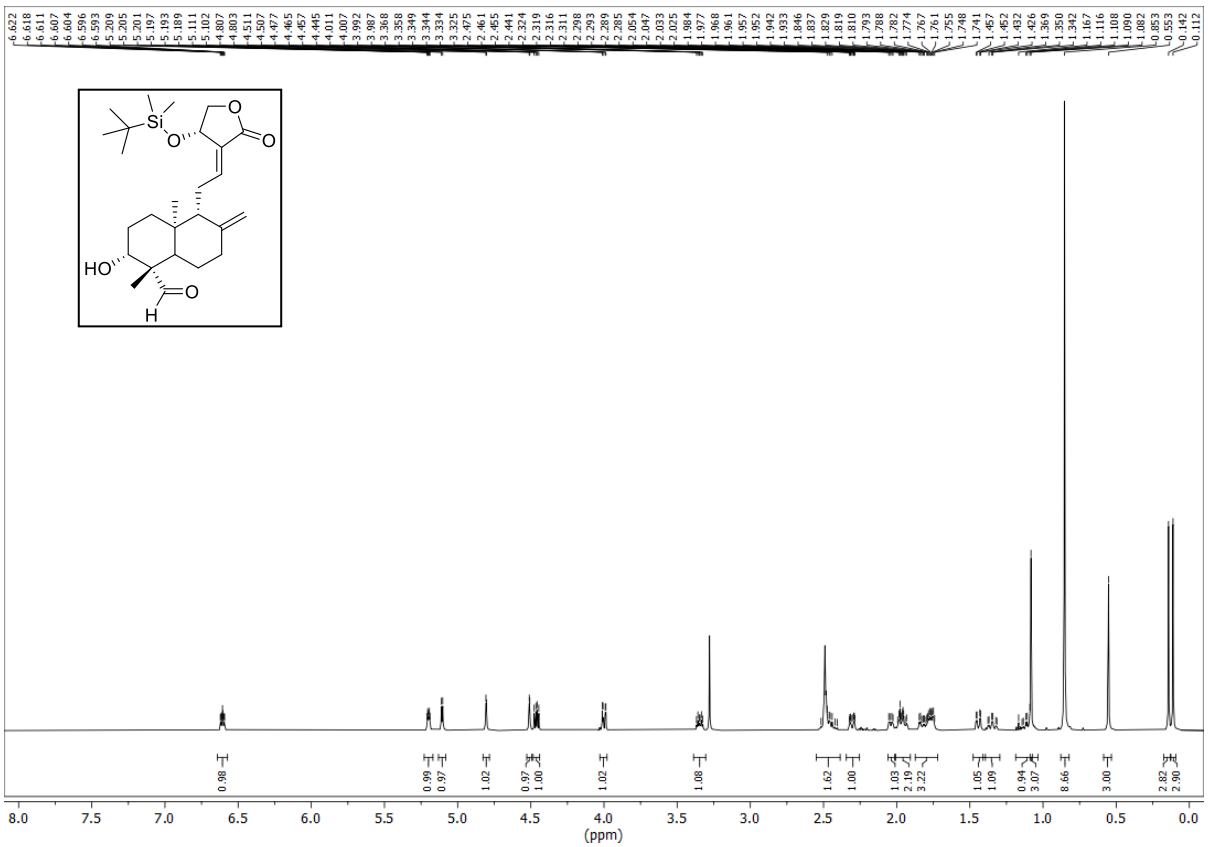

^{1}H NMR spectrum of **13**.

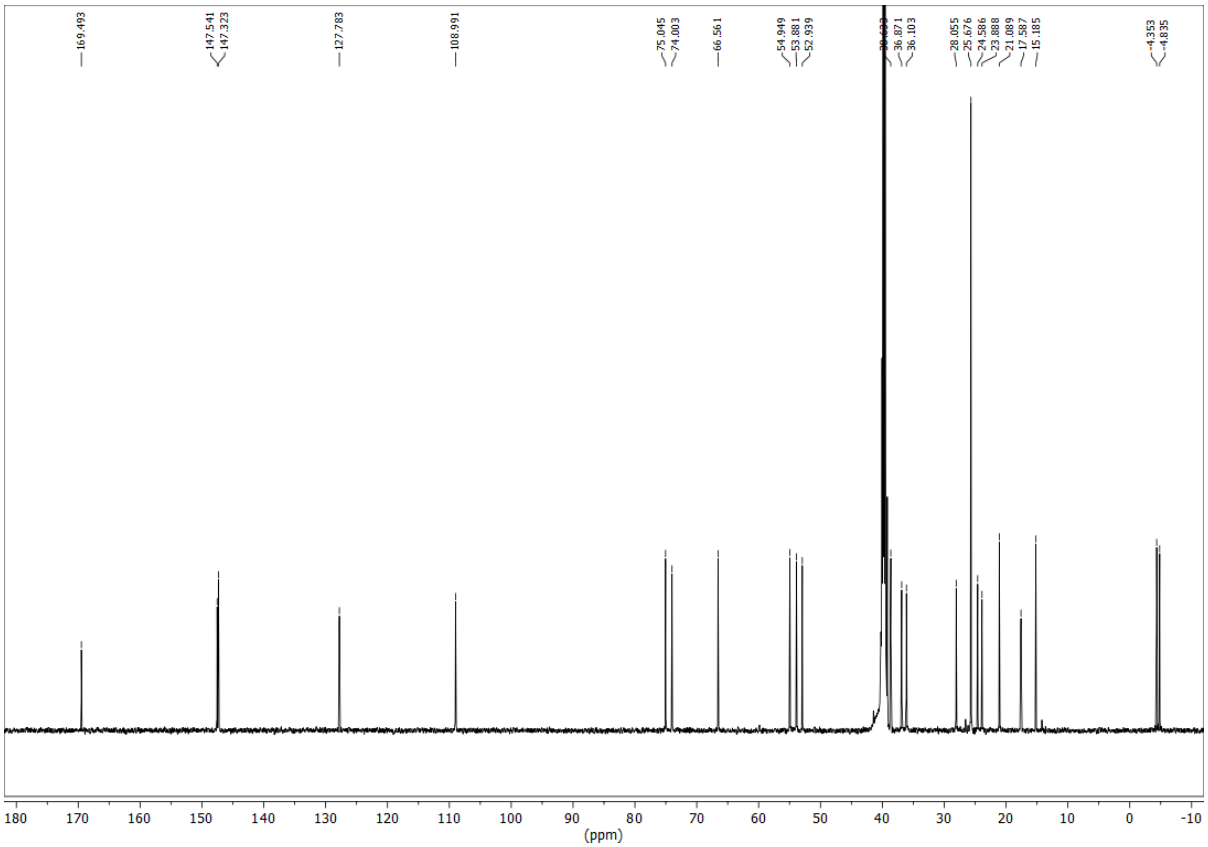

^{13}C NMR spectrum of **13**.

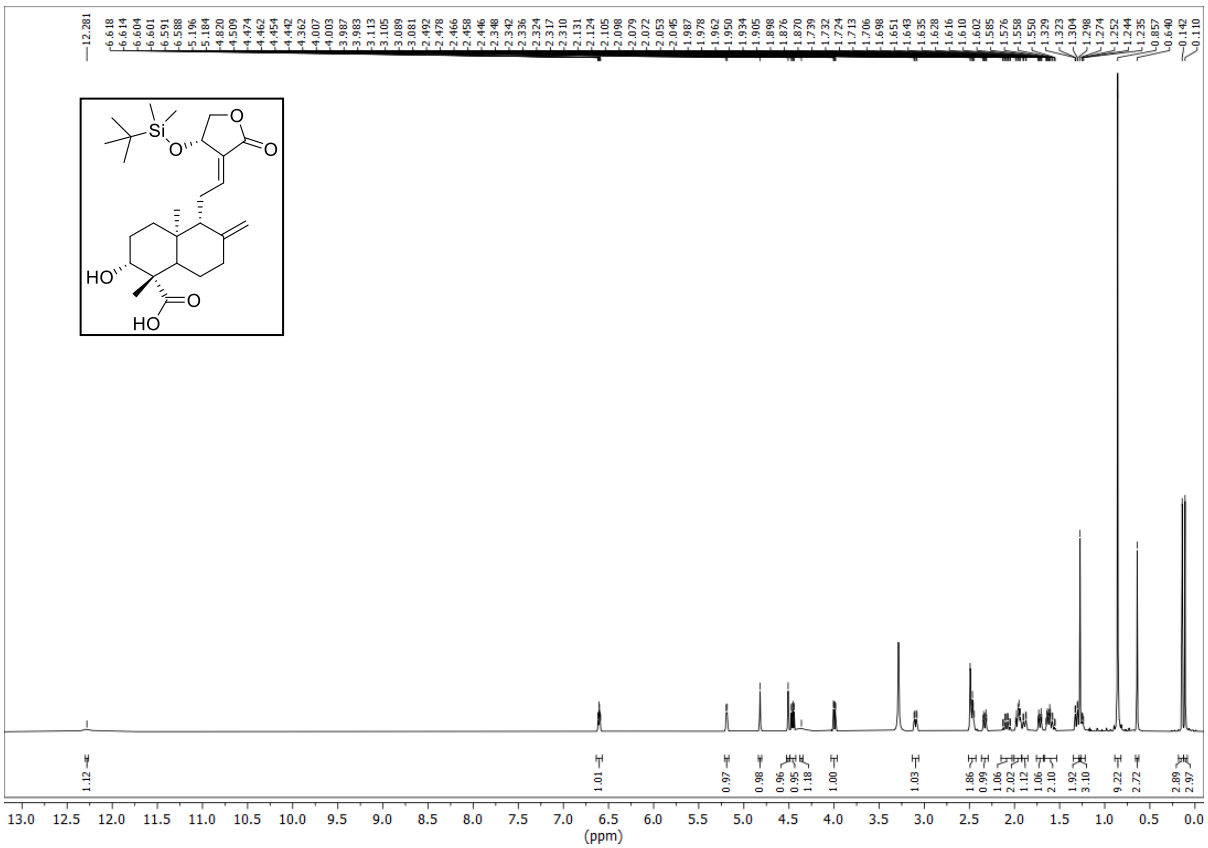

^{1}H NMR spectrum of **14**.

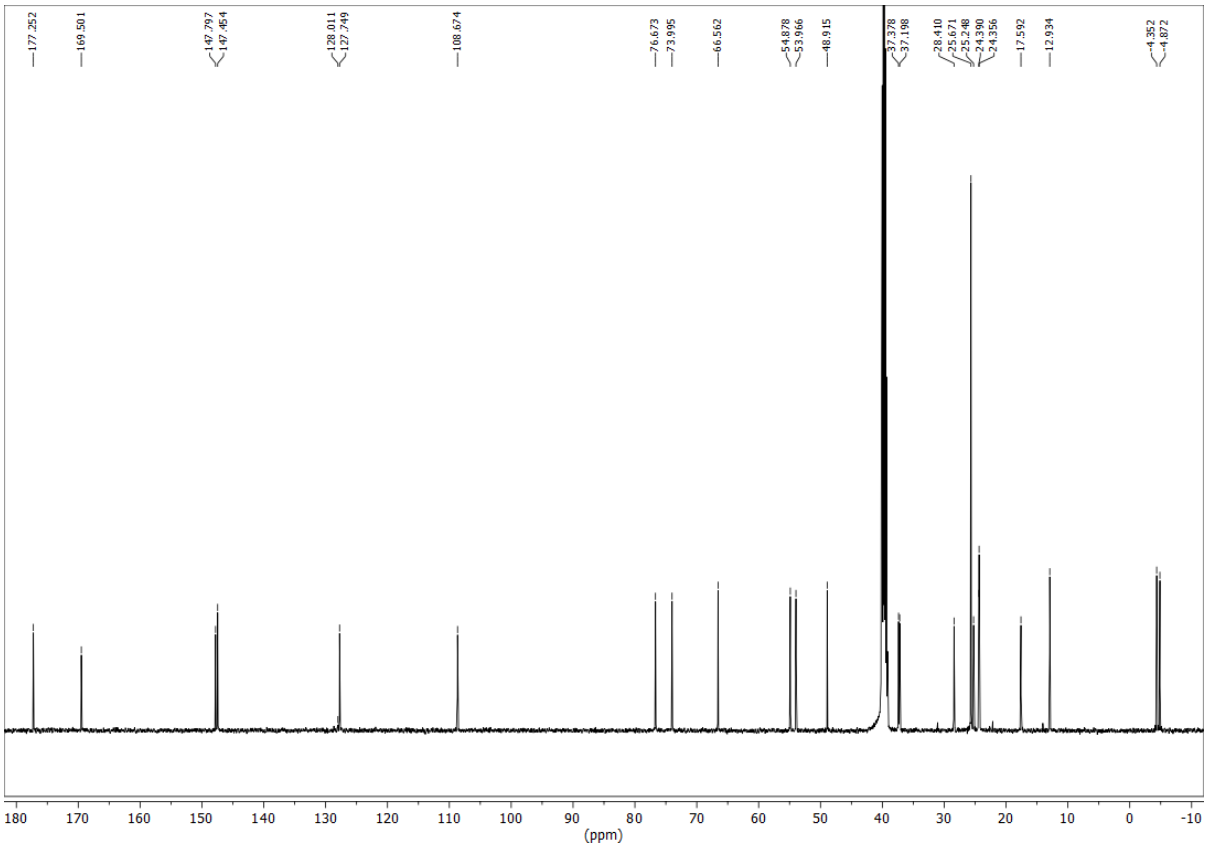

^{13}C NMR spectrum of **14**.

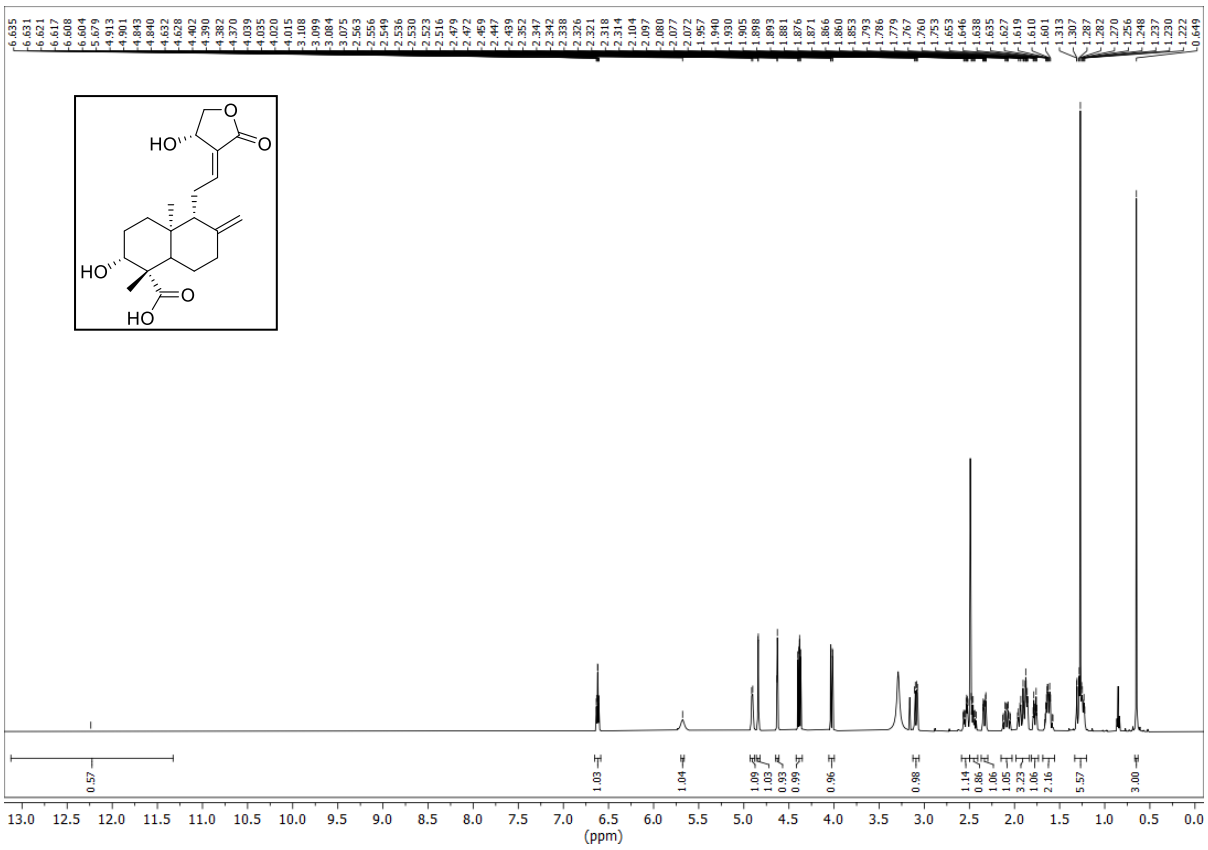

^{1}H NMR spectrum of **15**.

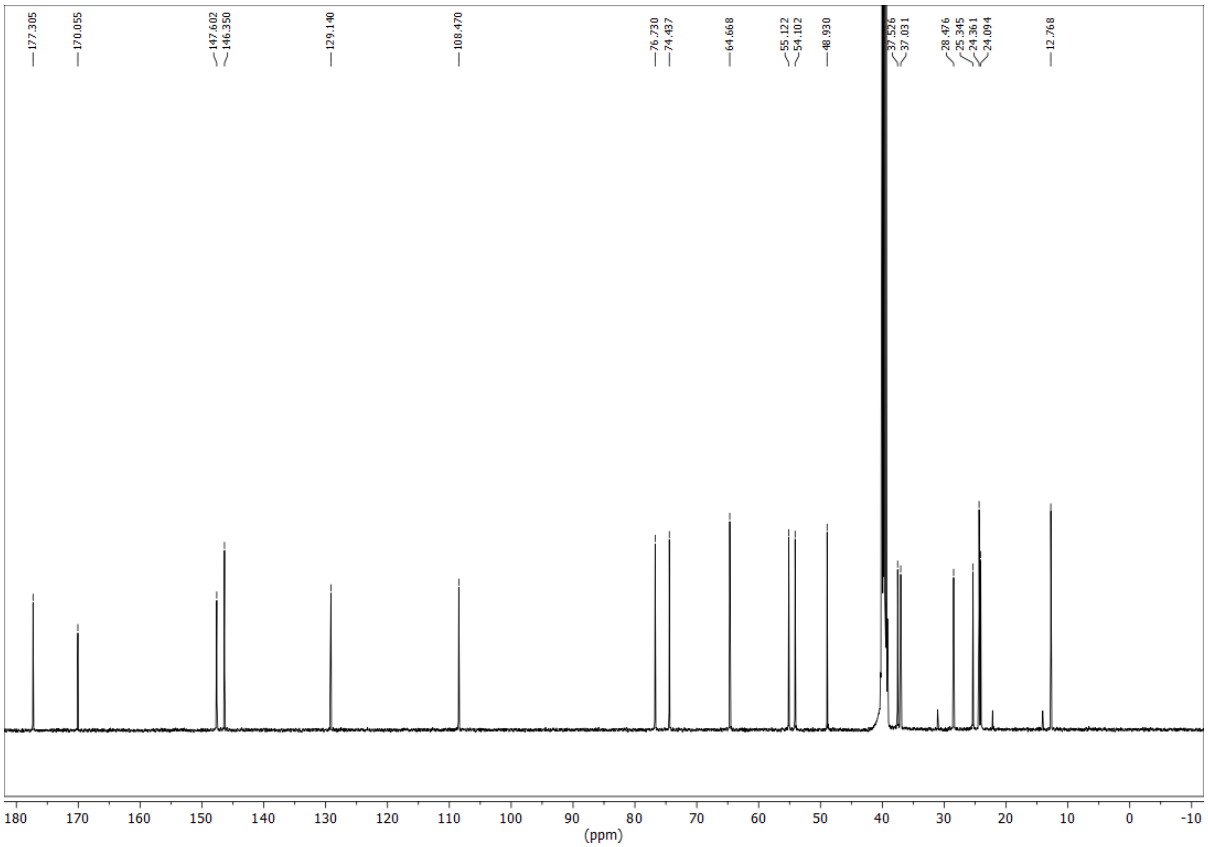

^{13}C NMR spectrum of **15**.

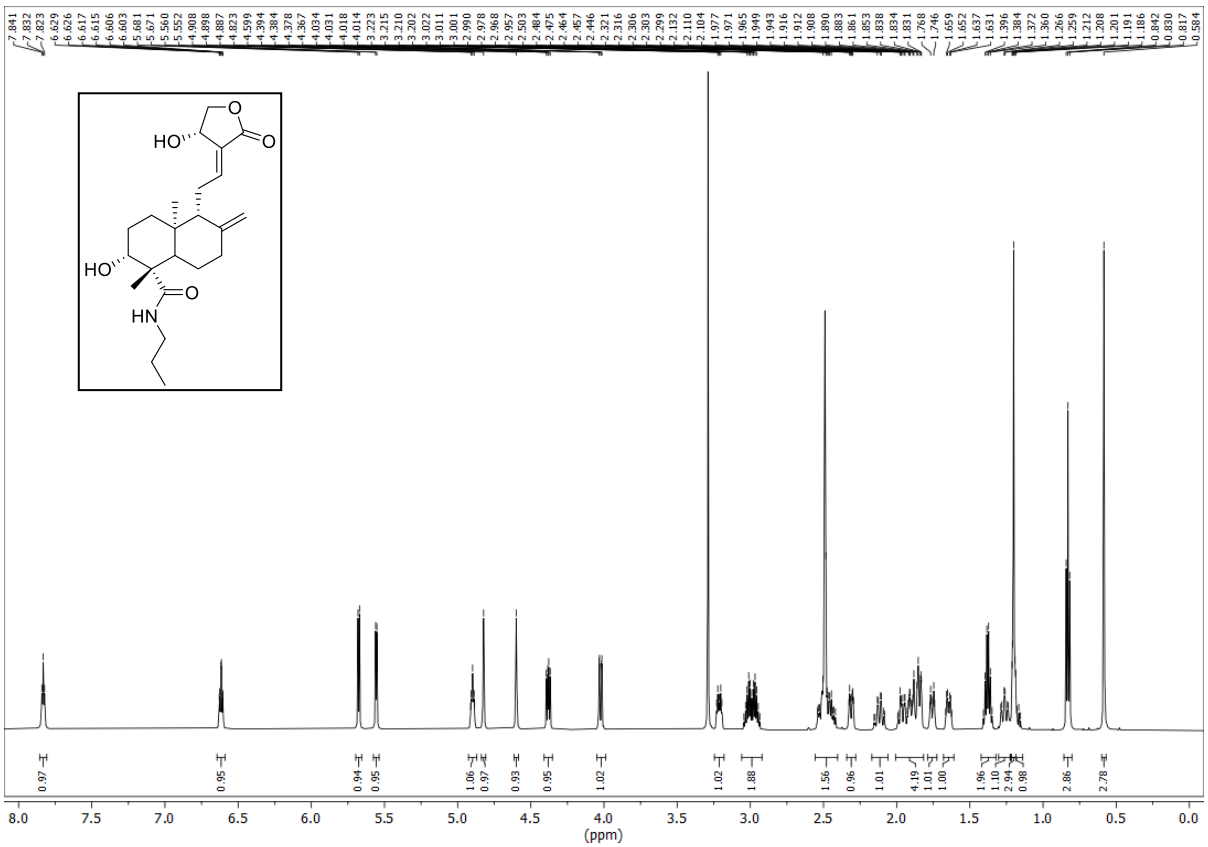

^{1}H NMR spectrum of **16a**.

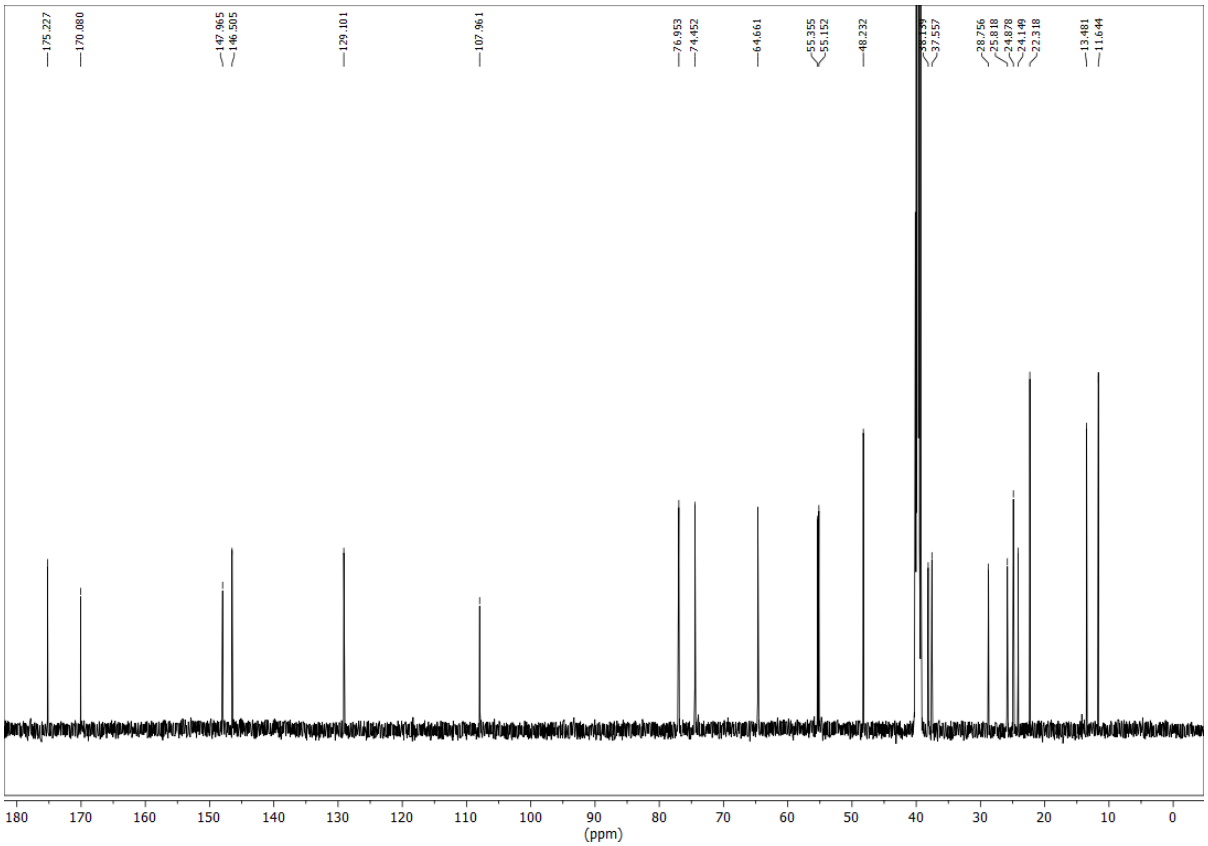

^{13}C NMR spectrum of **16a**.

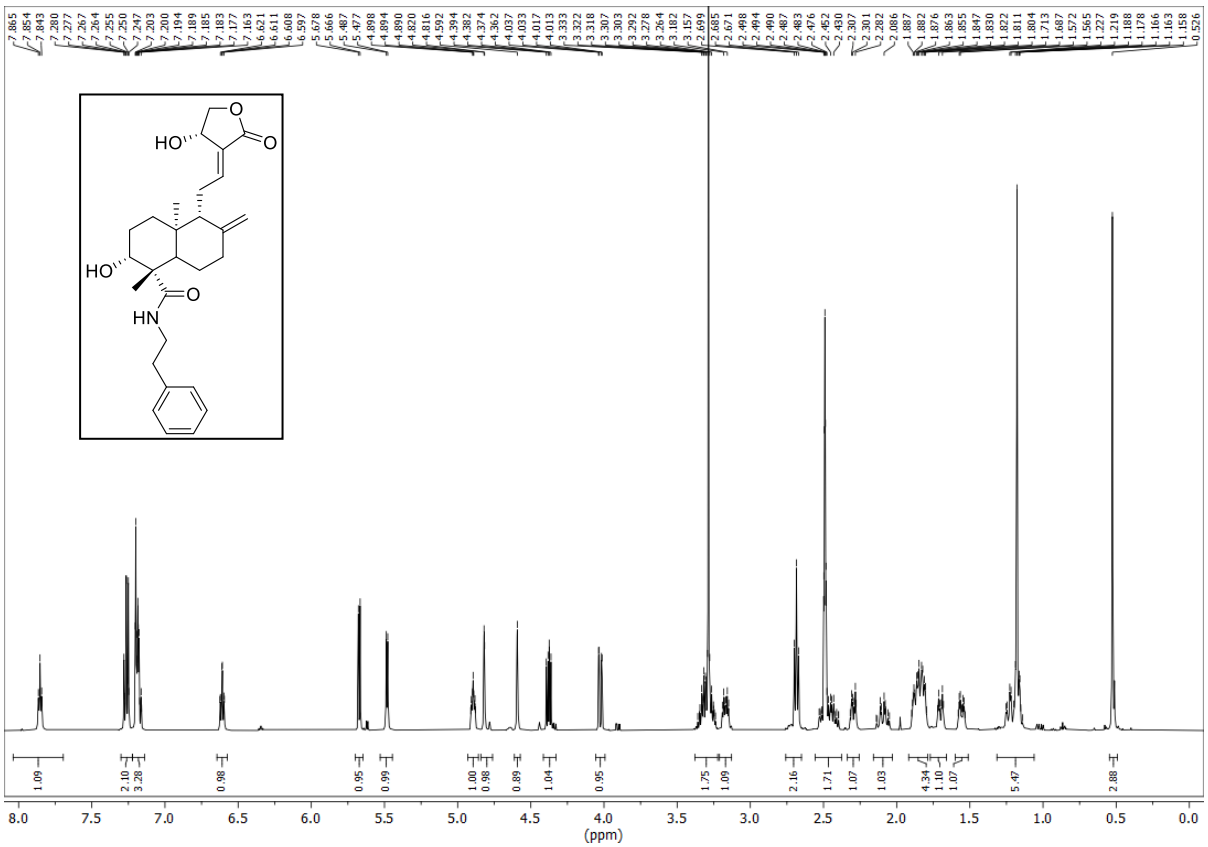

^{1}H NMR spectrum of **16b**.

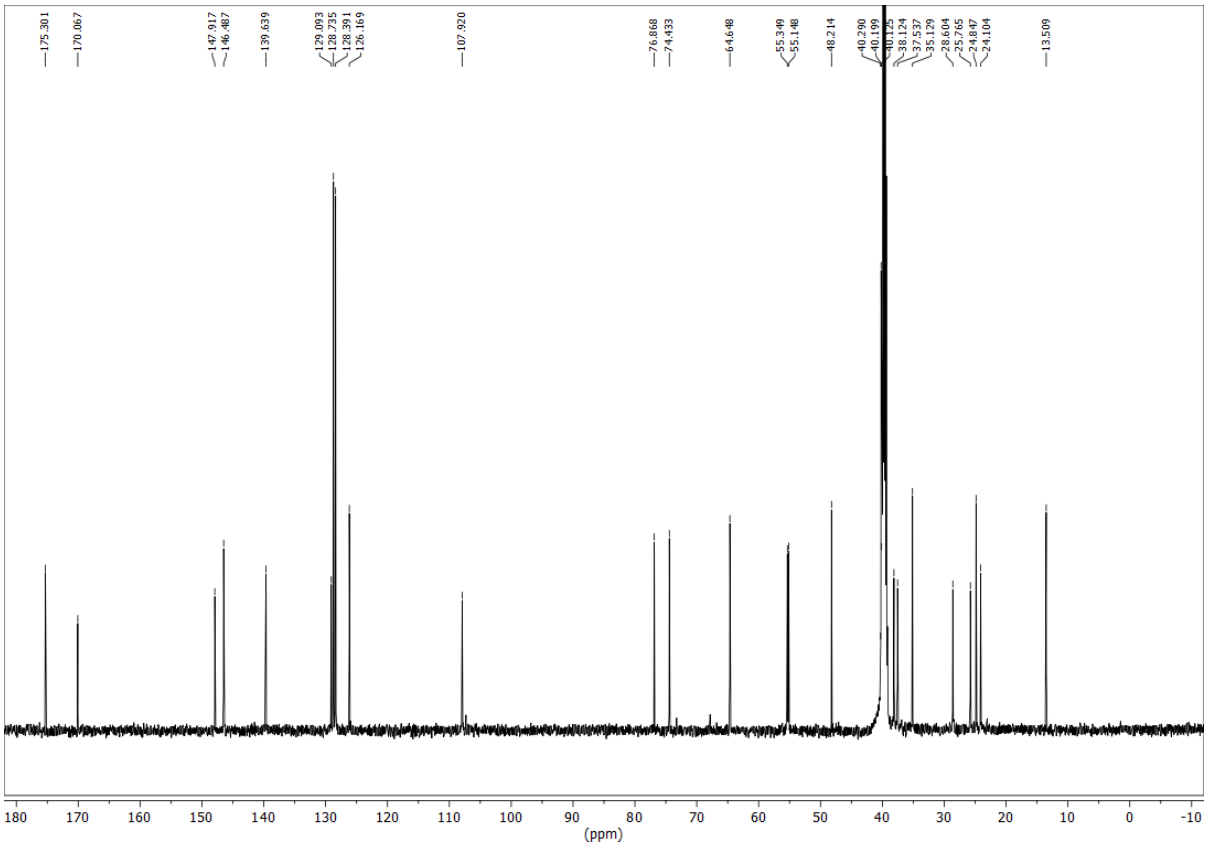

^{13}C NMR spectrum of **16b**.

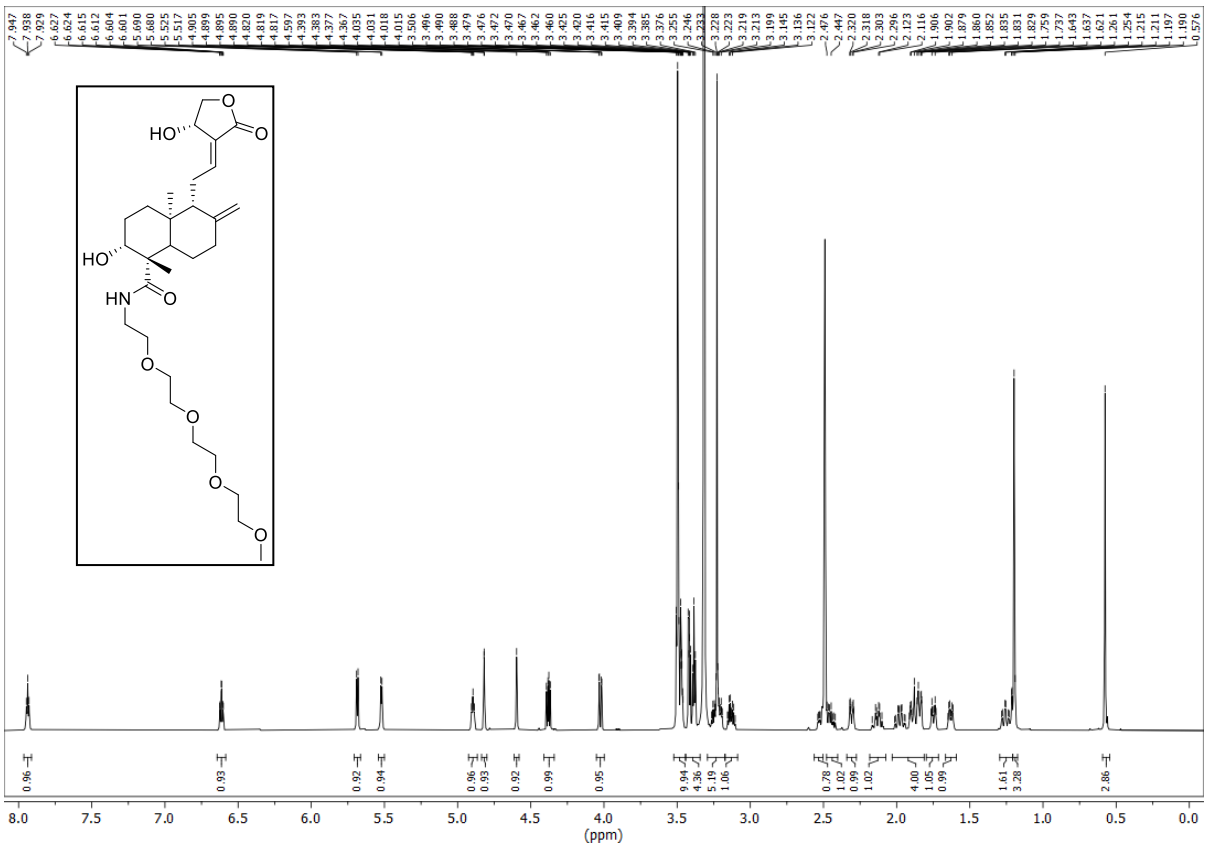

^{1}H NMR spectrum of **16c**.

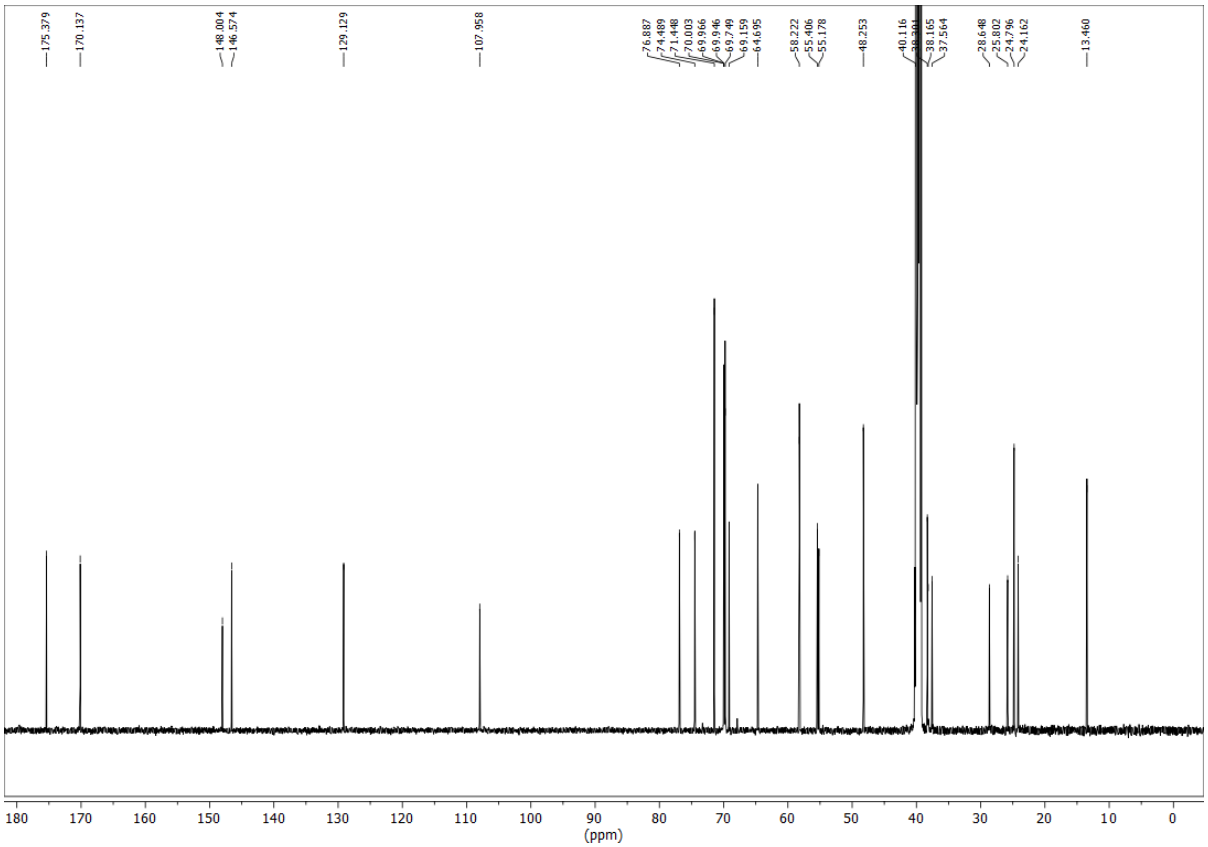

^{13}C NMR spectrum of **16c**.

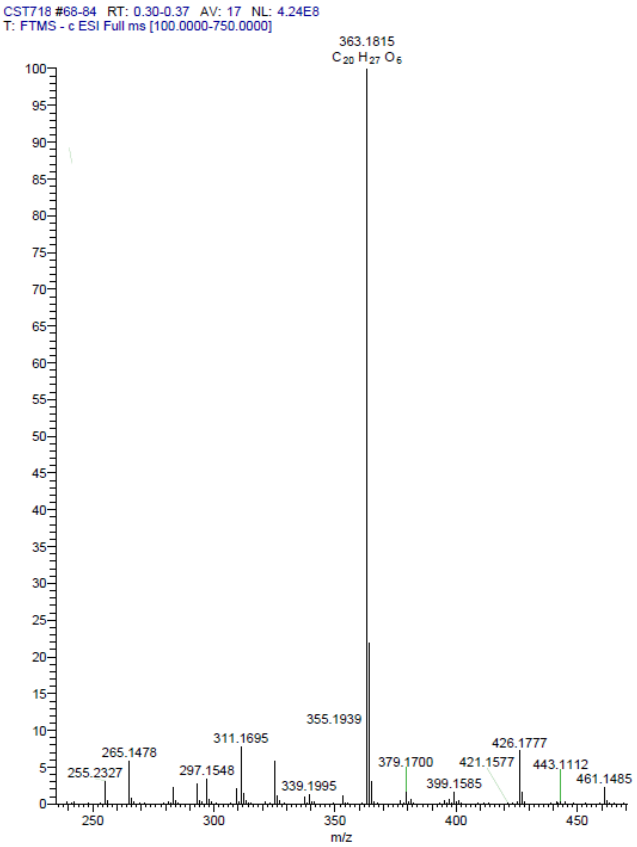

HRMS-ESI spectrum $[M–H]^-$ of **15.**

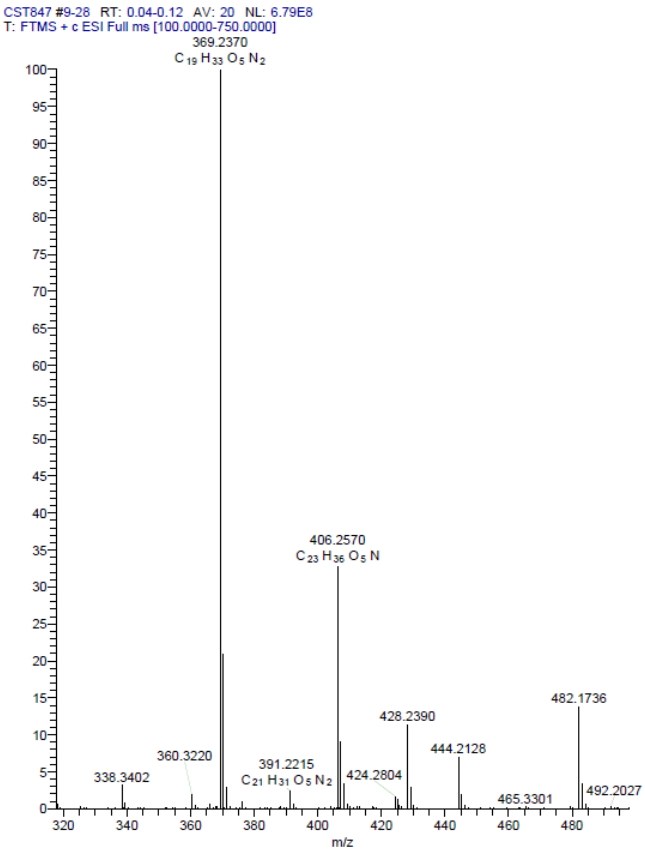

HRMS-ESI spectrum $[M+H]^+$ of **16a.**

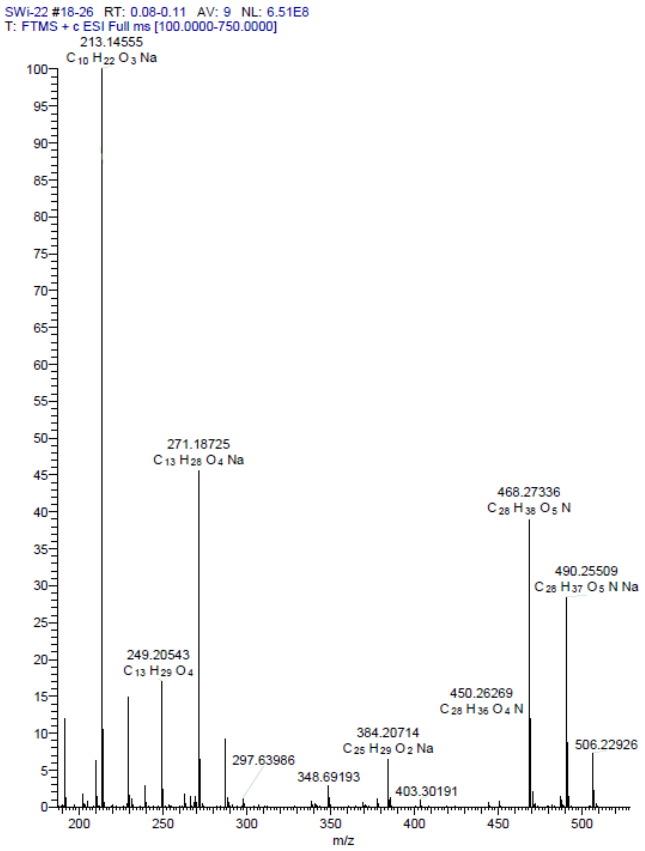

HRMS-ESI spectrum $[M+H]^+$ of **16b.**

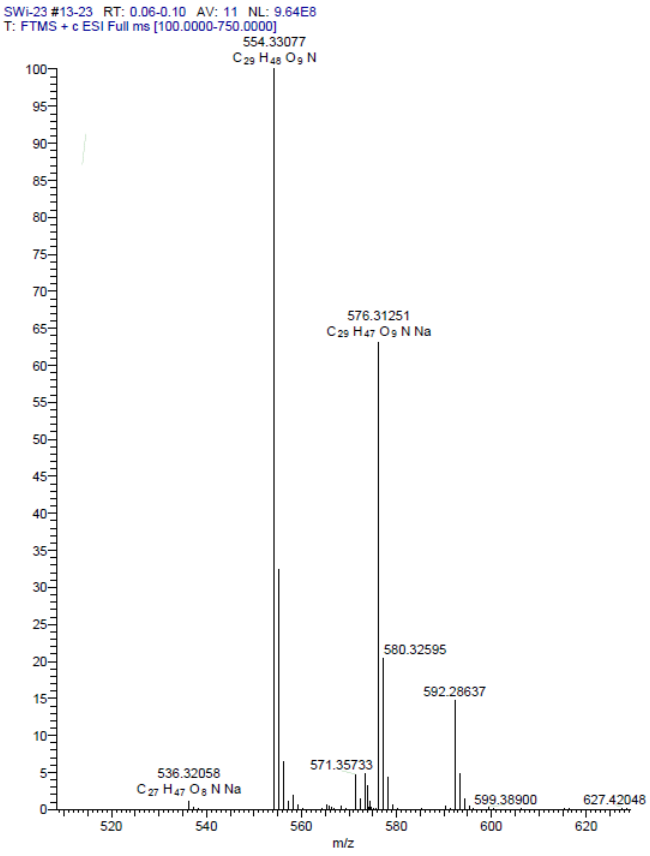

HRMS-ESI spectrum $[M+H]^+$ of **16c.**

References

(1) Steinebach, C., Ng, Y. L. D., Sosic, I., Lee, C.-S., Chen, S., Lindner, S., Vu, L. P., Bricelj, A, Haschemi, R., Monschke, M., Steinwarz, E., Wagner, K. G., Bendas, G., Luo, J., Gütschow, M., and Krönke, J. (2020) *Chem. Sci.* 11, 3474–3486.

(2) Kerns, E. H., Di, L., Petusky, S., Kleintop, T., Huryn, D., McConnell, O., and Carter, G. (2003) *J. Chromatogr. B* 791, 381–388.

(3) Valko, K., Nunhuck, S., Bevan, C., Abraham, M. H., and Reynolds, D. P. (2003) *J. Pharm. Sci.* 92, 2236–2248.

(4) Breidenbach, J., Lemke, C., Pillaiyar, T., Schäkel, L., Al Hamwi, G., Diett, M., Gedschold, R., Geiger, N., Lopez, V., Mirza, S., Namasivayam, V., Schiedel, A. C., Sylvester, K., Thimm, D., Vielmuth, C., Phuong Vu, L., Zyulina, M., Bodem, J., Gütschow, M., and Müller, C. E. (2021) Targeting the Main Protease of SARS-CoV-2: From the Establishment of High Throughput Screening to the Design of Tailored Inhibitors. *Angew. Chem. Int. Ed.* 60, 10423–10429.

(5) Escher, B. I., Glauch, L., König, M., Mayer, P., and Schlichting, R. (2019) Baseline Toxicity and Volatility Cutoff in Reporter Gene Assays Used for High-Throughput Screening. *Chem. Res. Toxicol.* 32, 1646–1655.

(6) Maeder, V., Escher, B. I., Scheringer, M., and Hungerbühler, K. (2004) Toxic Ratio as an Indicator of the Intrinsic Toxicity in the Assessment of Persistent, Bioaccumulative, and Toxic Chemicals. *Environ. Sci. Technol.* 38, 3659–3666.

(7) Escher, B. I., Dutt, M., Maylin, E., Tang, J. Y. M., Toze, S., Wolf, C. R., and Lang, M. (2012) Water Quality Assessment Using the AREc32 Reporter Gene Assay Indicative of the Oxidative Stress Response Pathway. *J. Environ. Monit.* 14, 2877–2885.

(8) Escher, B. I., Henneberger, L., König, M., Schlichting, R., and Fischer, F. C. (2020) Cytotoxicity Burst? Differentiating Specific from Nonspecific Effects in Tox21 *in Vitro* Reporter Gene Assays. *Environ. Health Perspect.* 128, 077007.

(9) Escher, B. I., Neale, P. A., and Villeneuve, D. L. (2018) The Advantages of Linear Concentration-Response Curves for in Vitro Bioassays with Environmental Samples: Linear CRCs. *Environ. Toxicol. Chem.* 37, 2273–2280.

(10) Wong, M. H. L., Bryan, H. K., Copple, I. M., Jenkins, R. E., Chiu, P. H., Bibby, J., Berry, N. G., Kitteringham, N. R., Goldring, C. E., O'Neill, P. M., and Park, B. K. (2016) Design and Synthesis of Irreversible Analogues of Bardoxolone Methyl for the Identification of Pharmacologically Relevant Targets and Interaction Sites. *J. Med. Chem.* 59, 2396–2409.

(11) Cava, M. P., Chan, W. R., Haynes, L. J., Johnson, L. F., and Weinstein, B. (1962) The Structure of Andrographolide. *Tetrahedron* 18, 397–403.

(12) Tang, C., Gu, G., Wang, B., Deng, X., Zhu, X., Qian, H., and Huang, W. (2014) Design, Synthesis, and Biological Evaluation of Andrographolide Derivatives as Potent Hepatoprotective Agents. *Chem. Biol. Drug. Des.* 83, 324–333.

(13) Jada, S. R., Subur, G. S., Matthews, C., Hamzah, A. S., Lajis, N. H., Saad, M. S., Stevens, M. F. G., and Stanslas, J. (2007) Semisynthesis and in Vitro Anticancer Activities of Andrographolide Analogues. *Phytochemistry* 68, 904–912.

(14) Liu, Z., Law, W.-K., Wang, D., Nie, X., Sheng, D., Song, G., Guo, K., Wei, P., Ouyang, P., Wong, C.-W., and Zhou, G.-C. (2014) Synthesis and Discovery of Andrographolide Derivatives as Non-Steroidal Farnesoid X Receptor (FXR) Antagonists. *RSC Adv.* 4, 13533–13545.

(15) Singh, D., and Chaudhuri, P. K. (2013) Reduction of Andrographolide and Its Stereostructure by NMR and X-Ray Study. *Nat. Prod. Res.* 27, 680–683.

(16) Song, Y., Xin, Z., Wan, Y., Li, J., Ye, B., and Xue, X. (2015) Synthesis and Anticancer Activity of Some Novel Indolo[3,2-b]Andrographolide Derivatives as Apoptosis-Inducing Agents. *European J. Med. Chem.* 90, 695–706.